Progress Report: 9/07-8/12

Title: Integrated Nondestructive Spatial and Chemical Analysis of Lignocellulosic Materials during Pretreatment and Bioconversion to Ethanol

ID: ER64499-1030816-0013824

Principal Investigator: Gary Peter,
Co-PIs: Stephen Blackband, Lonnie Ingram, Richard Yost

Proposed Objectives:

The *objectives* of this proposal are to 1) use advanced high resolution magnetic resonance microscopy (MRM), micro and nano x-ray computed tomography (x-ray CT), electron microscopy and imaging mass spectrometry (IMS) by matrix assisted laser desorption ionization (MALDI) ion trap mass spectrometry (MS) to quantify changes in the structure, porosity, pore size, interconnectivity, chemical organization and composition of grass and particularly woody materials during pretreatment and enzymatic degradation, and 2) integrate the results from these different quantitative imaging methods into a model for disassembly of the plant cell wall during pretreatment and bioconversion. Our *central hypothesis* is that integrating functional information about cell wall permeability measured by MRM, with cell wall density/thickness and structural changes measured with micro and nano-cat, scanning electron microscopy, and changes in chemical wall organization and composition obtained with IMS will lead to a quantitative description of changes in cell wall organization during pretreatment and enzyme mediated degradation.

Results

Executive Summary:

Excellent progress was made in standardizing three complementary methods: Magnetic resonance imaging, x-ray micro CT, and MALDI imaging linear ion trap mass spectroscopy to image biomass and chemical, anatomical and functional changes that occur during pretreatment and hydrolysis. Magnetic resonance microscopy provides excellent images with as low as 5 uM resolution with hydrated biomass samples. We visualized dramatic changes in signal associated with the hydrolysis of the carbohydrates by strong acids. Quantitative diffusion approaches were used to probe more subtle structural changes in biomass. Diffusion tensor calculations reflect diffusion anisotropy and fractional anisotropy maps clearly show the longer range diffusion within the vessels compared to within the fiber cells. The diffusion is increased along the cell walls of the vessels. Suggesting that further research with NMR imaging should be pursued. X-ray CT provides excellent images at as low as 3.5 uM resolution from dried biomass. Small increases in surface area, and decreases in local density have been quantified in with wood after mild pretreatments; these changes are expected to be underestimates of the hydrated wood, due to the ~12% shrinkage that occurs upon drying untreated wood. MALDI-MS spectra show high ion intensities at most mass to charge ratios in untreated and pretreated woody material. MALDI-MS^n is required to improve specificity and reduce background for imaging. MALDI-TOF is not specific enough for carbohydrate identification. Using MALDI-

LIT/MS^n we can readily identify oligomeric glucans and xylans and their fragmentation patterns as well as those of the glucuronic acid side chains of birch 4-O-methyl glucuronxylan. Imaging of glucan and xylan oligomers show that many contain isobaric ions with different distributions, indicating again that MS^n is needed for accurate imaging of lignocellulosic materials. We are now starting to integrate the three imaging methods by using the same set of biomass samples imaged with all three methods, and using common analytical software to quantify parameters from the three dimensional images.

In addition to the proposed experiments, we conducted imaging studies with a novel TOF-SIMS instrument available through collaborations with the AMOLF goup led by Ron Heeren at the FOM Institute in Amersterdam, Netherlands. ToF-SIMS was used to image intact cross sections of Populus stems with high spatial resolution, chemically selectivity. ToF-SIMS images were correlated with fluorescence microscopy which allowed for more positive ion identification.

Four peer reviewed publications resulted from this project.

Gustin, J., Jackson, S., Williams, C., Patel, A., Baier, J., Armstrong, P., Edwards, J.W., Peter, G.F., Settles, A.M., 2013. Analysis of maize (Zea mays) kernel density and volume using x-ray micro-computed tomography and single-kernel near infrared spectroscopy. *Agriculture and Food Chemistry* 61 10872-10880.

Hunter, C.T., Kirienko, D.H., Sylvester, A.W., Peter, G.F., McCarty, D.R., Koch, K.E. 2012. Cellulose synthase-Like D1 is integral to normal cell division, expansion and leaf development in maize. *Plant Physiol*. 158: 708-724.

Joshi, C.P., Thammannagowda, S., Fujino, T. Gou, J., Avci, U., Haigler, C.H., McDonnell, L.M., Mansfield, S.D., Menghesa, B., Carpita, N.C., Harris, D., DeBolt, S., Peter, G.F. 2011. Perturbation of wood cellulose synthesis causes pleiotropic effects in transgenic aspen. *Molecular Plant* 4: 331-45

Lunsford, K.A., Peter, G.F., Yost, R.A., Direct Matrix-Assisted Laser Desorption/Ionization Mass Spectrometric Imaging of Cellulose and Hemicellulose in *Populus* Tissue. 2011. Anal Chem. 83: 6722-30.

SPECIFIC AIM 1: Characterize and quantify changes in signal characteristics induced by pretreatment and during enzymatic degradation with magnetic resonance microscopy

Using 5mm rf coils, 39uM MR images have been collected from *Populus*, pine and bagasse stems. These images are of excellent quality and show the expected anatomy of the materials. Interestingly, the lignified secondary walled xylem cells of the vascular bundles of bagasse appear quite dark compared with the primary cell walled cells within the mesophyll region (**Figure 1-1**) (***Note***: all **Figures** are placed at the end of each section). This low relaxation signal within the vascular bundle is attributed to the lower free water present in the dense lignified xylem cells compared with the nonlignified thin primary cell walls of the mesophyll.

As a first test, commercially available *Populus* wood chips were incubated in 60% sulphuric acid conditions known to hydrolyze the carbohydrate polymers to monomeric sugars. **Figure 1-2** quantifies the dissolution of carbohydrate materials with increasing time determined from MRM

T2 images acquired at 39 uM resolution. The advancing boundary from the surface to the interior of the chips can is clearly visualized indicating that MRM imaging can successfully detect changes in biomass caused by strong acid. Preliminary accounts of this work have been published in our National High Magnetic Field Laboratory (NHMFL) yearly reports (distributed internationally) and we are submitting a manuscript describing these results to the Journal of Magnetic Resonance Imaging. These preliminary data are quite encouraging that the gross microstructure of wood chips can be visualized.

This resolution limitation with the acquisition was overcome with new microcoils that are 50-500 microns in diameter. These state of the art rf microcoils greatly improve the signal to noise ratio (SNR) and we recently validated their utility by being the first to publish MR images of individual rat brain cells (1). Using these new microcoils we acquired the highest resolution MR images obtained to date of wood (**Figures 1-4** and **1-5**). With the improved SNR a much better delineation of the wood chip microstructure is evident, and this is comparable with high resolution x-ray CT microscopy, except in the images are acquired in a fully hydrated state. We are extremely excited with this new capability and technique and are moving forward with a series of experiments to quantify changes in the wood chips after pretreatment and digestion. **Figure 1-6** shows our first experiments in these regards, where a clear change in the wood chip microstructure is evident after mild acid pretreatment.

Previously, work at high temperatures demonstrated significant signal changes in wood chip samples as a function of time with digestion in acid. Although the results were significant, such high temperatures (which were used to accelerate the digestion process) are not used commercially. When the temperature was lowered to commercial standards, signal changes were no longer observed. In response, we improved the MR with a two pronged approach – the first was integration of new microcoils and second implementation of quantitative diffusion approaches as a means of more precisely probe the subtle structural changes that occur during digestion. These quantitative approaches are more rigorous than the qualitative approaches proposed in the project.

For quantitative diffusion imaging, a series of scans are acquired with diffusion encoding in several different directions. From this data, the diffusion tensor can be calculated, which reflects the diffusion anisotropy within materials. These techniques are used in human MRI for a variety of applications, but mostly to map fiber tracts in the brain. Within the wood chip, diffusion occurs preferentially along, rather than across, the xylem/phloem vessels. *Our hypothesis is that this anisotropy will degrade with wood chip digestion and de-lignification*. In the following we summarize our results.

Figure 1-7 shows the resultant fractional isotropy (FA) map that is quantitatively generated. Blue represents no anisotropy (as seen in the water surrounding the wood chip), while within the chip there is considerable anisotropy (red and yellow speckling). Data were acquired with TR/TE=1000/23.6, FOV=0.8 cm, in-plane resolution=31 μm, slice thickness = 0.5 mm, diffusion time (Δ)=10 msec, b-value =700 s/mm^2, and at a temperature of 23°C. Note the blue regions in the wood chip, which represents the isotropic diffusion of the relatively unrestricted water within the xylem vessels.

From the MR image, the xylem vessels appear to be at least 50-100 um in diameter. Therefore, in the 10 msec diffusion time, most molecules (except those very close to the vessel wall) will not travel far enough to encounter the vessel wall and will experience free diffusion. The presence/absence of lignin will thus have a negligible effect. To increase the sensitivity to diffusion, we lengthened the diffusion time to 25 msec, and increased the sample temperature to 40°C. At 40°C, the diffusion coefficient of water, D, is ~0.003 mm^2/s. With the higher temperature and longer diffusion time, the root-mean-square displacement of water molecules is about 12 µm. This is still substantially smaller than the xylem vessel diameter, but we anticipate that some anisotropy will be detectable near the vessel edges. **Figure 1-8** shows the effect of this improvement. The xylem vessels are more clearly defined (blue holes) and there is increased anisotropy at the edges of the vessels (demonstrated by the light blue vessel framing).

FIGURES FOR AIM 1:

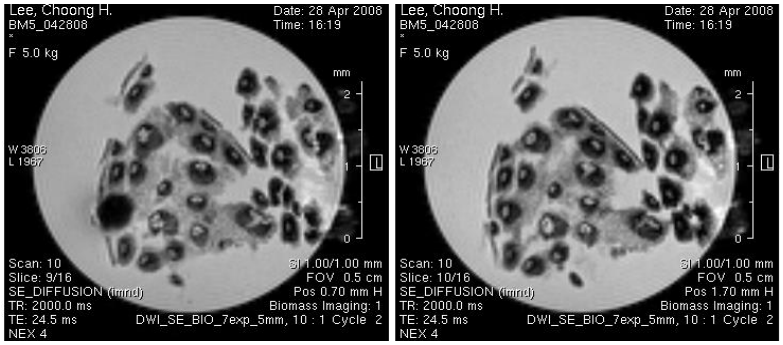

Figure 1-1: 39 uM diffusion weighted images of bagasse stems, cross sectional face. Dark ellipses correspond to lignified vascular bundles and gray material between vascular bundles are stem parenchyma cells.

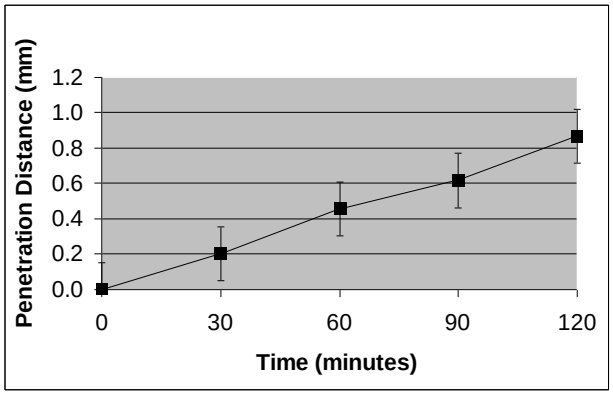

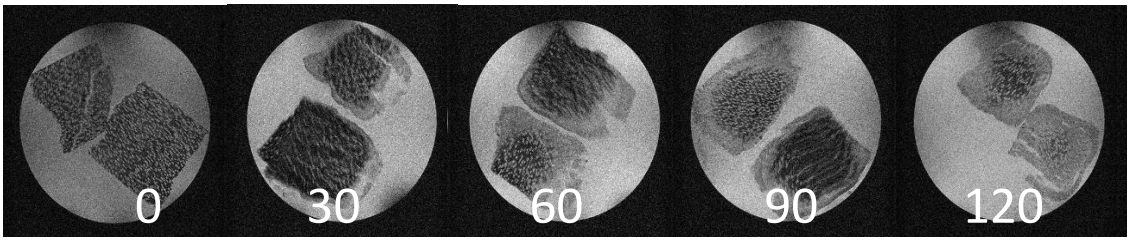

Figure 1-2. A time course of the average sample penetration of determined from the hyperintense signal in the wood chips as a function of the time after exposure to 60% sulphuric acid (with standard error bars). The same wood samples were used at each time point and boiled for 20 minutes in water before imaging. The penetration distance is an average of eight measurements from a central image slice on each chip made at roughly equidistant spacing around the sample. The image insert shows example images from two chips at each time point.

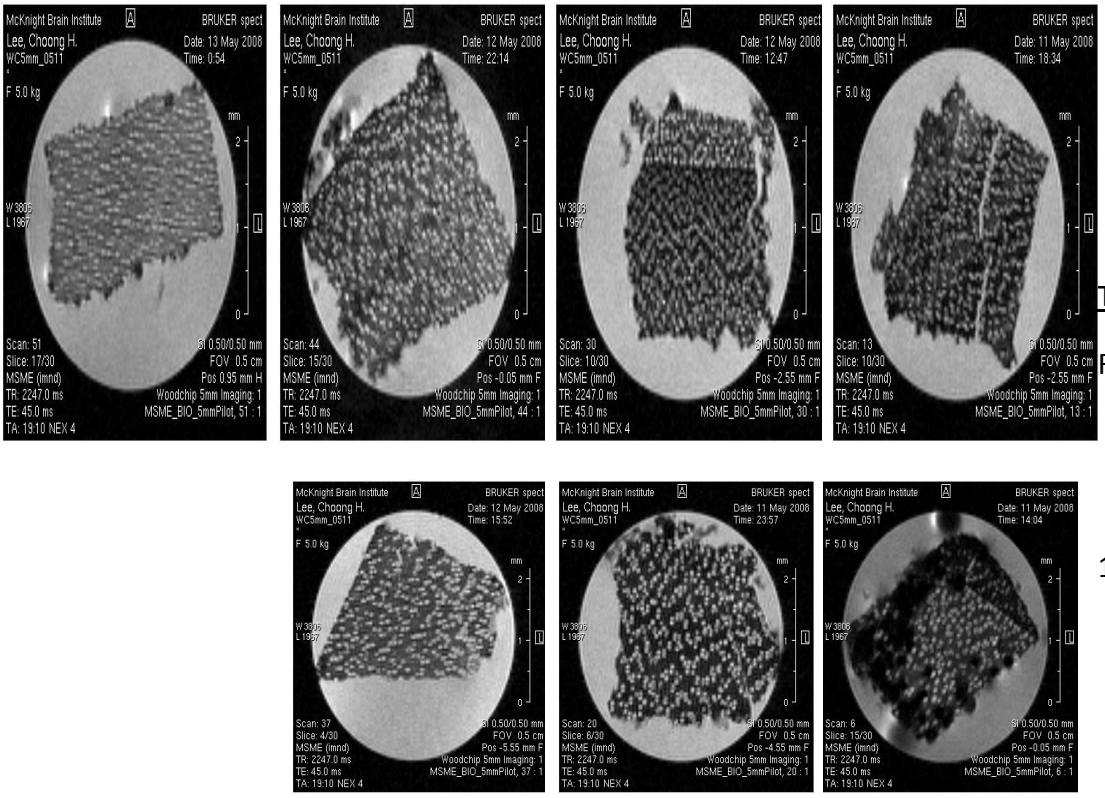

Figure 1-3: MRM images of wood chips after various levels mild acid pretreatment. Chemical analysis shows that 3% sulphuric acid is sufficient to remove hydrolyze of the xylan and release it from the chips. Dark spots in the 3% H_2SO_4 + 145^oC image are air bubbles. Little difference in the signal is observed across the chips or between different treatments.

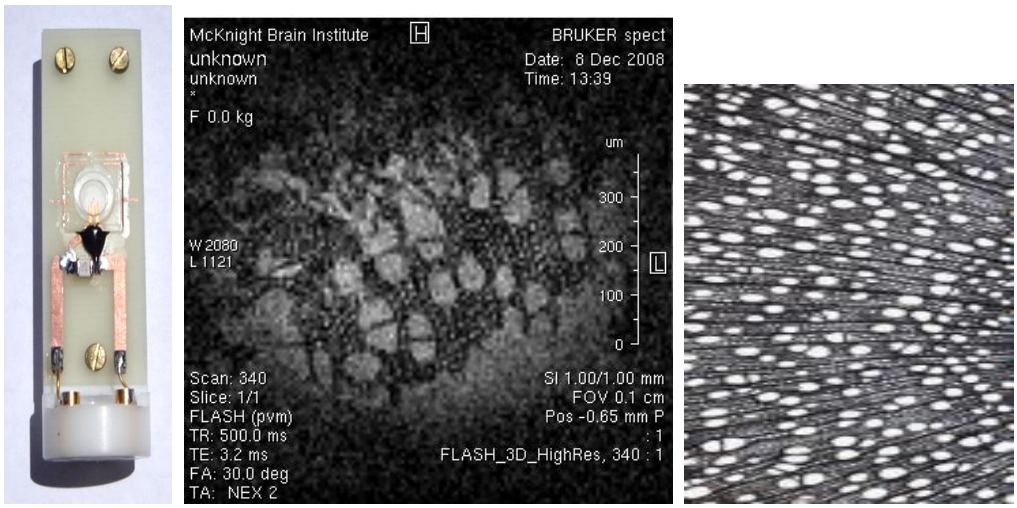

Figure 1-4. Using the new rf micrcoils (left) this figure shows an MR microimage (8 microns, 4hrs 33 min) of a wood chip sample (middle) with example optical histology 5X objective.

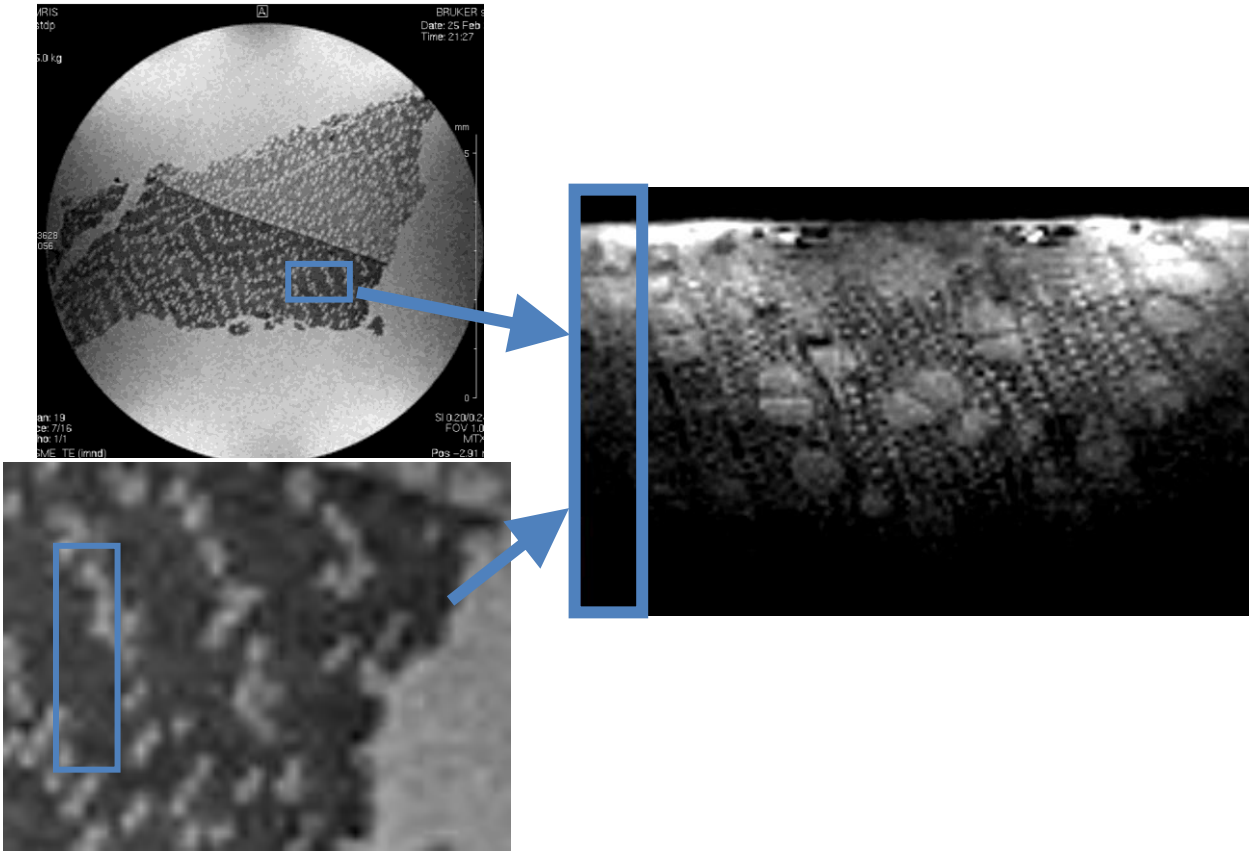

Figure 1-5. Illustration of the microcoil SNR improvement. On the left is a conventional 40micron resolution image (top) with an expanded view (bottom). Using a microcoil an 8 micron image (right) with an equivalent field of view (indicated by the boxes) is show – the clear improvement in the ability to see the wood microstructure is evident.

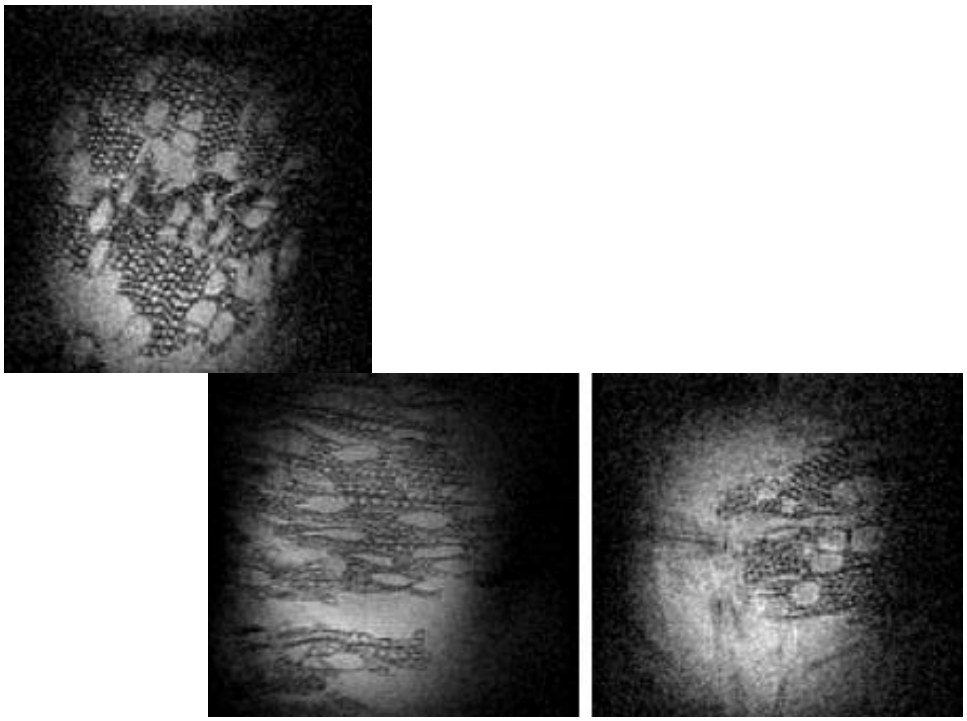

Figure 1-6. Microimages (8 microns resolution) of wood chips in (from left to right) 0.5, 2 and 3.5% acid at 145^{o}C. Note the deterioration of the microstructure with exposure. Each image acquired in 4hrs 33 minutes.

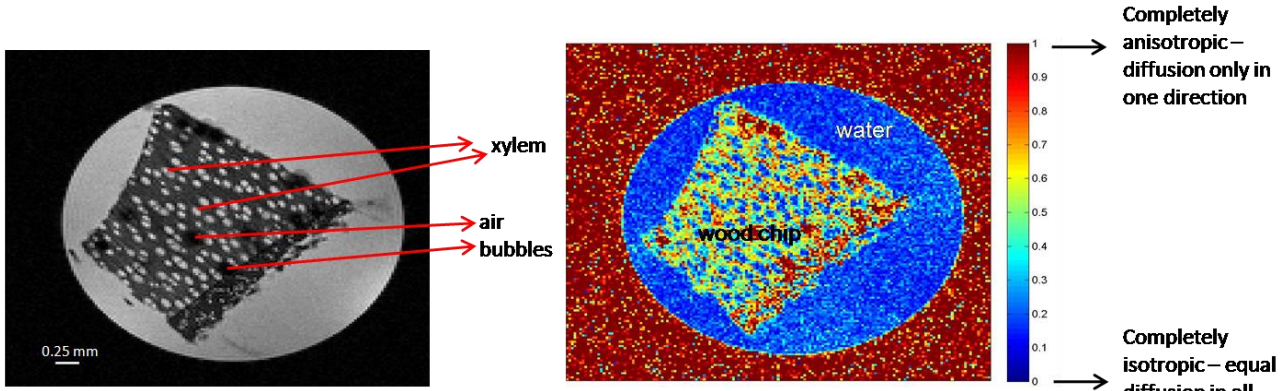

Figure 1-7. Left: conventional qualitative image. Right: calculated fractional anisotropy map of water diffusion from diffusion tensor MRI.

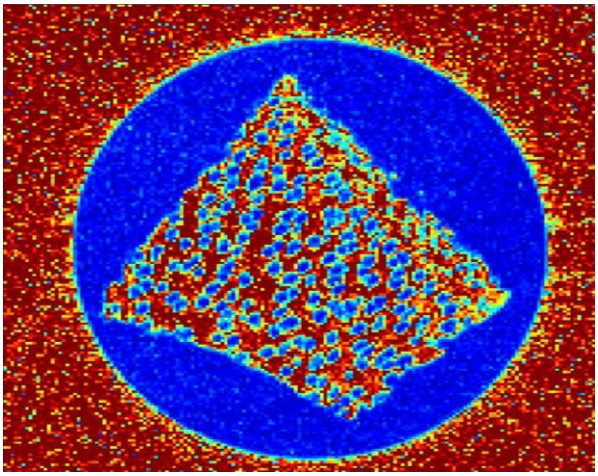

Figure 1-8. Wood chip FA map with the diffusion sensitivity improved. The vessels are clearly defined (blue holes). TR/TE=2000/35.6, FOV=0.6 cm, in-plane resolution=31 µm, slice thickness = 1.0 mm, 19 averages, diffusion time (Δ)=25 msec, b-value =900 s/mm2, temp=40°C.

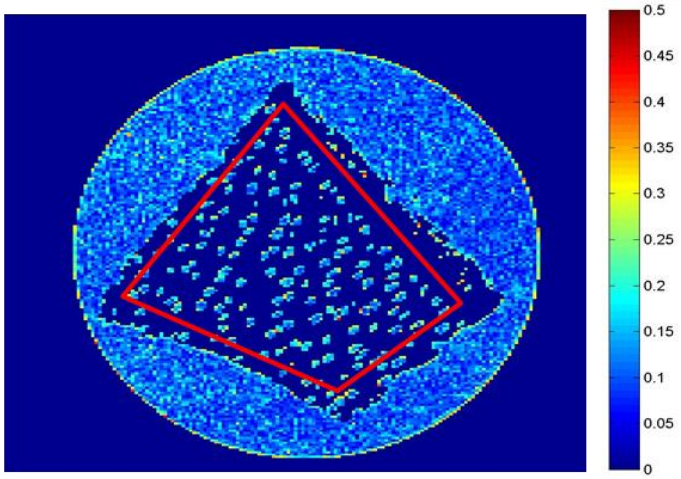

Figure 1-9. A similar FA map, but with all the non-xylem tissue segmented out. The water in the xylem only is evident, and increased anisotropy can be seen at the edges of the xylem.

SPECIFIC AIM 2: Quantify changes in biomass architecture, density, cell wall thickness, porosity and surface area induced by pretreatment and during enzymatic degradation with micro and nano x-ray computed tomography and electron microscopy

An x-ray micro-CT 35 was purchased from Scanco Medical AG using funds from this project and funds from an NSF award to Gary Peter. Using this instrument, we have successfully imaged dried woody and grass biomass. **Figure 2-1** shows typical 3D images of wood from balsa and oak scanned at 6.0 uM per voxel and reconstructed. High quality images, sufficient for quantification are readily obtained from dry biomass materials. Analysis of 3D models for cell wall thickness and airspace are readily computed using algorithms developed for trabecular bone analyses. Balsa is known to be a very low density wood and oak a high density wood. The mean wall thickness is 17 $\pm$ 0.004 uM of balsa is less than half that found for oak 39.1 $\pm$ 0.072 uM; whereas, the mean airspace size in balsa is 24.0 $\pm$ 0.007 uM significantly higher than in oak 19.3 $\pm$ 0.01 uM. The cell wall thickness and the vessel diameters determined from x-ray

CT images are consistent with those obtained by optical microscopy of dehydrated wood. For example, in *Populus*, single wall thicknesses average 4.5-5.0 uM for the fiber cells and the diameter of vessels averages 30-40 uM. **Figure 2-2** shows typical 3D images of *Populus* wood scanned at 3.5 uM per voxel and reconstructed. High quality images, sufficient for quantization are readily obtained from dry biomass materials. The cell wall thickness and the vessel diameters determined from x-ray CT images are consistent with those obtained by optical microscopy of dehydrated wood. For example, in *Populus*, single wall thicknesses average 4.5-5.0 uM for the fiber cells and the diameter of vessels averages 30-40 uM.

We quantified differences in density, *Populus* wood surface area and porosity, cell wall thickness compared untreated with wood pretreated using 3.5% sulphuric acid and 145^{o}C, conditions that we have determined extract the 15-18% of the xylan that is typically present in wood. Images of the pretreated wood appear somewhat less structured (**Figure 2-2**); this is consistent with the appearance of these samples which are more brittle and brown. After pretreatment, wood density was reduced by 6.5% and cell wall thickness was on average 2% lower; whereas, surface area and surface area to volume ratio both increased by 2%. These changes in biomass structure are significant and are all in the direction expected. However, they underestimate the percent changes that occur in fully hydrated wood, because wood shrinks significantly upon drying. We compared the volume of untreated wood samples when they were fully hydrated and dried (5% moisture content) measured in the micro CT. We found a 12% decrease in wood volume when it was dried. This 12% decrease occurred in the radial and tangential planes but not in the longitudinal plane parallel to the fiber cells. Our shrinkage results are the same as those reported previously with much larger samples of *Populus* wood. Thus, if the shrinkage of pretreated wood is similar to untreated wood, then changes in wall thickness, surface area and surface area to volume ratio are expected to be more than 10% greater in hydrated wood.

Figure 2-3, (upper left) shows typical images of sugarcane bagasse stem tissue. Interestingly, in addition to the vascular bundle cells being readily visualized in bagasse stems, the parenchyma cell walls are clearly detectable. **Figure 2-3** (lower left) shows an image of the recalcitrant bagasse material left after full processing of bagasse into ethanol at the UF pilot cellulosic bioethanol facility. The process used to convert sugarcane bagasse to ethanol is one being scaled up towards commercialization by Verenium Corp. and involves a mild acid soak and steam gun pretreatment followed by cellulase digestion and co-fermentation with bacterial biocatalysts (L. Ingram, unpublished). The recalcitrant material left after conversion is principally composed of tightly associated, lignified vascular bundles (VB) with little to no primary cell walled parenchyma cells. Although, the recalcitrant VBs appear quite intact, due the lignin remaining in the middle lamellae region still holding the cells together tightly in the bundles, the x-ray CT analyses show that substantial degradation has occurred. This degradation is apparent in the Figure 2-3 images where the pretreated VB has thicker walls and the recalcitrant VB has more and larger air space. The images also show that the material was removed/degraded only on the exterior surface of the VB. In contrast, the cells closest to the the interior vessel elements, which are normally filled with water, were not significantly affected, suggesting that enzyme penetration was substantially less or limited by diffusion into the vessel

elements. Quantification using a local adaptive threshold, indicated a ~32% increase in cell wall surface to volume ratio in the recalcitrant versus pretreated VBs.

One limitation of x-ray CT imaging of wood is that the density of the lignocellulosic wall is very similar to the density of water, thus limiting the ability to threshold for image analysis when the air spaces are filled with water. We are exploring four approaches to image wood when the walls are near saturation: 1) to remove water from the wood with a gentle vacuum prior to imaging, 2) to hydrate the walls after drying by incubating in a high humidity environment that swells the wood without introducing unbound or free water, 3) introducing contrast agents, including high density nanoparticles and polymerizing silicone agents used for CT imaging in mammals, and 4) close comparisons with the MRM, this alternative will be discussed more in Aim 4.

FIGURES FOR AIM 2

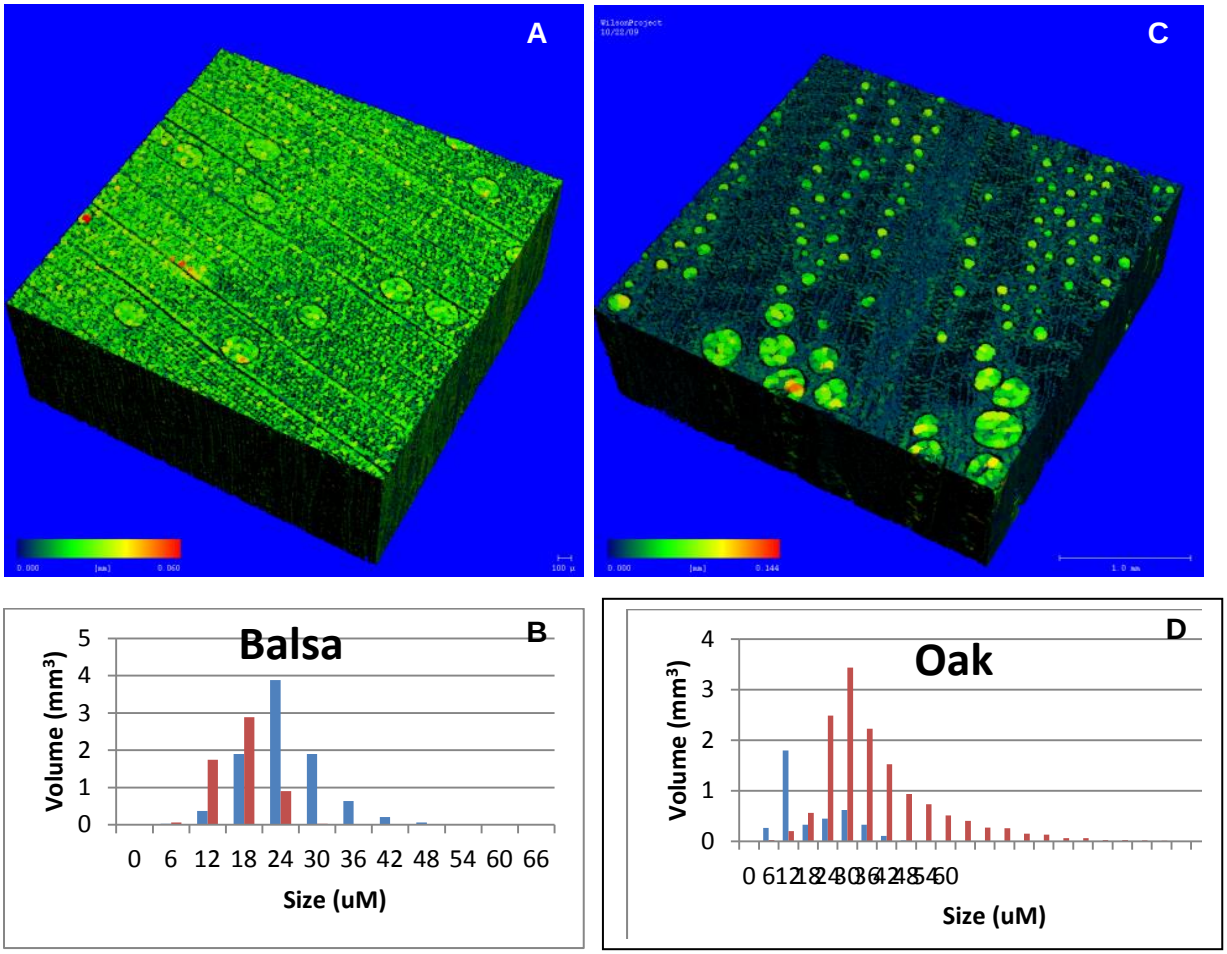

Figure 2-1: x-ray micro-CT analysis of wood with dramatically different densities. A) 3D image of balsa wood showing the size of the airspace,with brighter colors indicating larger airspaces. B) frequency distribution of size of the airspace (blue) and wall thickness (red) for balsa wood, C) 3D image of oak wood showing the size of the airspace, D) frequency distribution of size of the airspace (blue) and wall thickness (red) for oak wood.

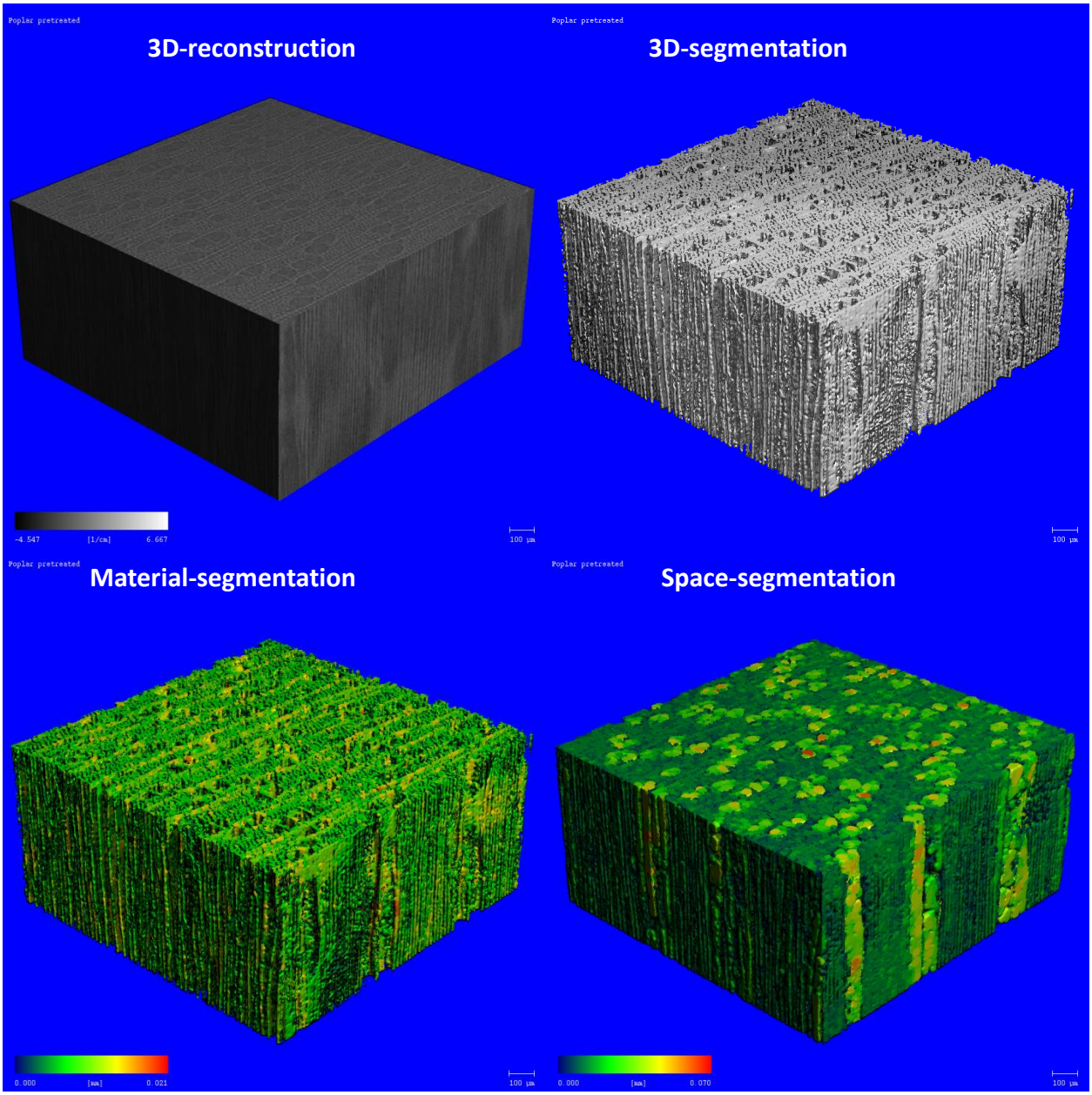

Figure 2-2 shows typical 3D images at 3.5 uM per voxel acquired at 45kV of *Populus* wood, thresholded for cell wall material versus air. The bottom colored images shows the local dimensions of the cell wall material on the left and the air space on the right.

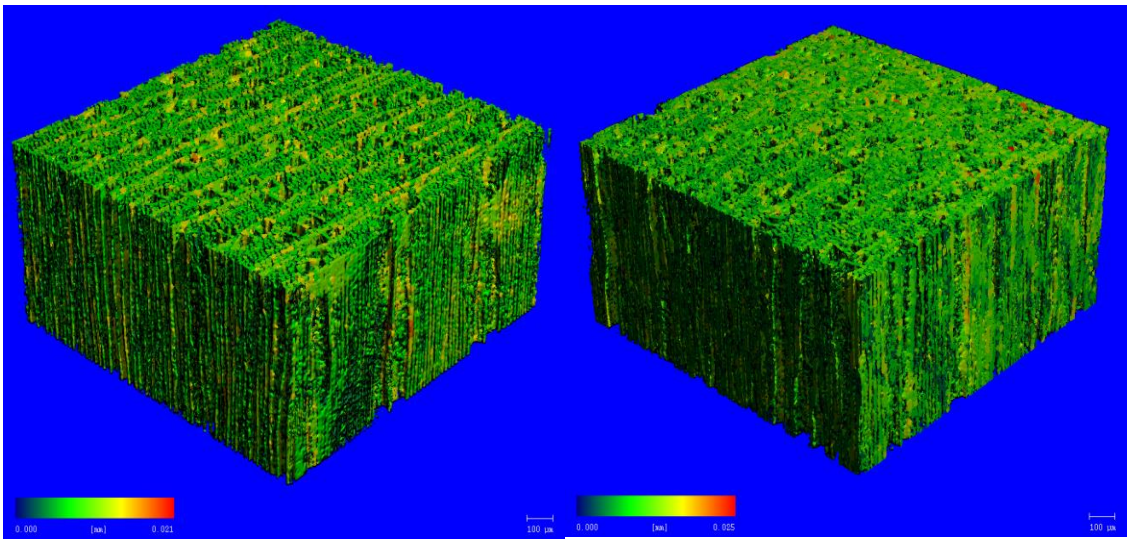

Figure 2-3. 3D images at 3.5 uM per voxel acquired at 45kV of *Populus* wood before and after pretreatment. The image of the pretreated wood has less distinct shaped cells especially in the upper half of the image, indicating a loss of order.

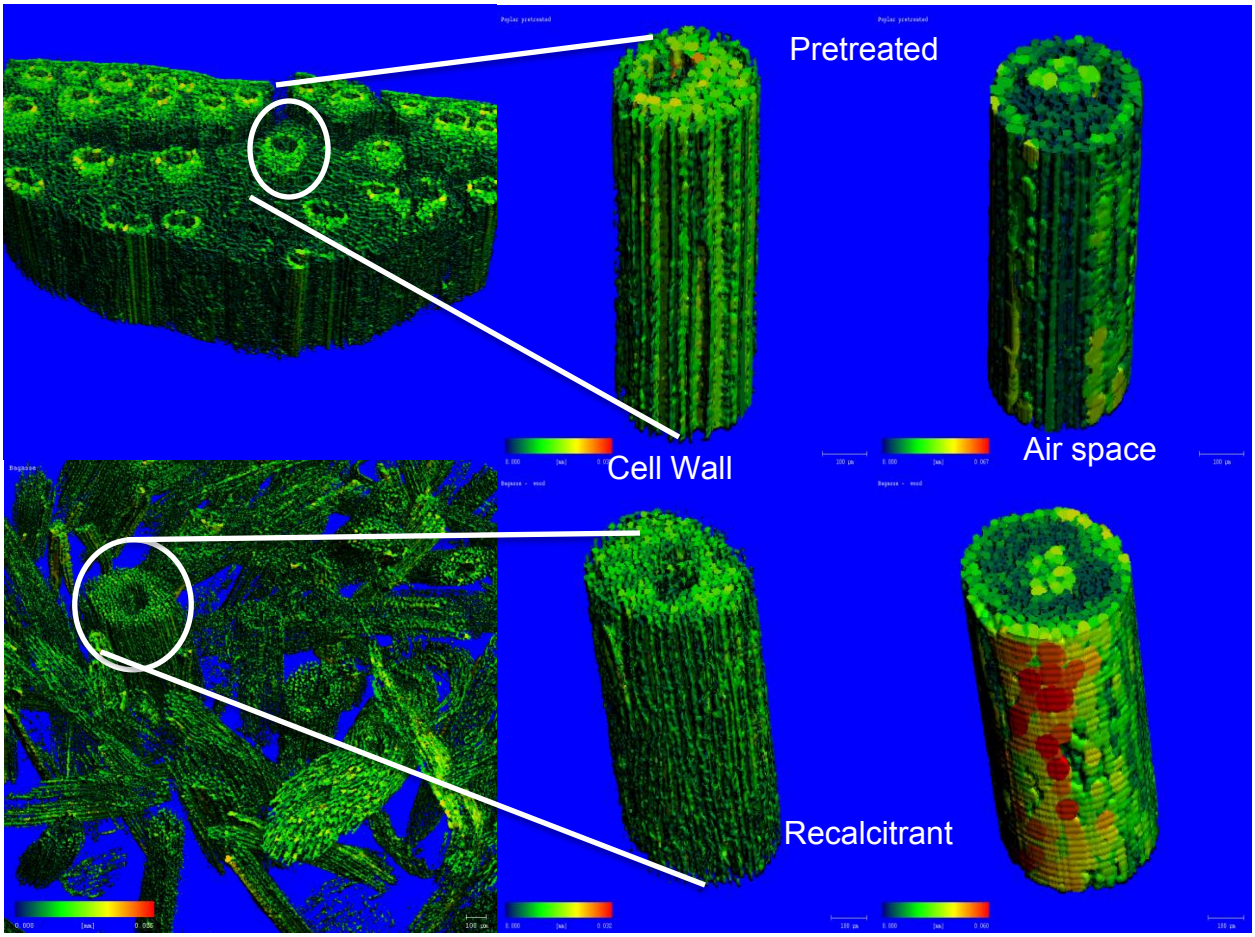

Figure 2-4. Typical 3D images at 3.5 uM per voxel acquired at 45kV of pretreated sugarcane bagasse (top) and recalcitrant sugarcane bagasse left after bioconversion to ethanol (bottom), The images were analyzed with a local adaptive thresholding algorithm to distinguish cell wall material (center) from air space (right). The brighter yellow and red colors indicate larger size spheres can fit into the local cell wall or air space. The process used to convert sugarcane bagasse to ethanol is one being scaled up towards commercialization by Verenium Corp. and involves a mild acid soak and steam gun pretreatment followed by cellulase digestion and co-fermentation with bacterial biocatalysts (L. Ingram, unpublished). The recalcitrant material left after conversion is principally composed of tightly associated, lignified vascular bundles (VB) with little to no primary cell walled parenchyma cells. Although, the recalcitrant VBs appear quite intact, due the lignin remaining in the middle lamellae region still holding the cells together tightly, the x-ray CT analyses clearly show that substantial degradation has occurred. This hydrolysis is seen in the images where pretreated VBs have thicker walls and the recalcitrant VB has more and larger air space (Figure 2-4).

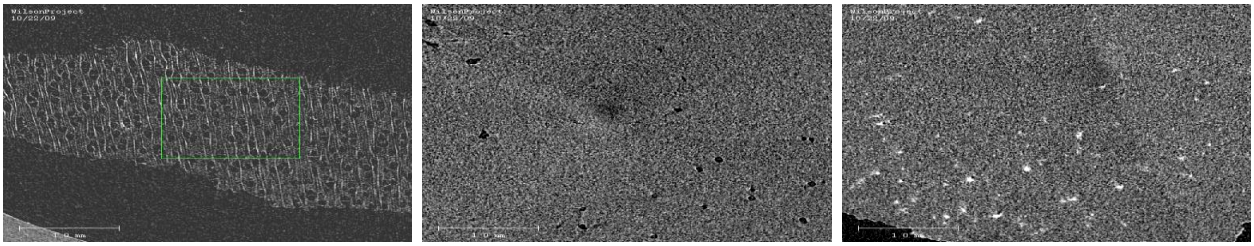

Figure 2-5: Initial test with gold nanoparticles to contrast vessel lumen in wet wood. A) Typical slice of dried poplar wood, showing good contrast between air in the vessel lumen and fiber and ray cells. B) Slice of wet wood before application of gold nano-particles, showing limited contrast between water filled vessels and fiber and ray cells. C) Slice of wet wood after infusion of gold nanoparticles, showing the bright white particles in the vessels of wet wood.

Although not directly related to the goals of this project, in collaboration with other colleagues we used x-ray micro CT to analyze the density, anatomical and cell wall changes in mutants of cellulose biosynthesis in *Populus,* cellulose synthase like D1 in maize, and demonstrated for the first time the ability to calibrate Near Infrared Spectroscopy for maize kernel density. These publications demonstrate the utility of using x-ray micro CT imaging for characterizing biomass and cell wall formation. The citations and abstracts of these publications acknowledge funding of this award.

Gustin, J., Jackson, S., Williams, C., Patel, A., Baier, J., Armstrong, P., Edwards, J.W., Peter, G.F., Settles, A.M., 2013. Analysis of maize (Zea mays) kernel density and volume using x-ray micro-computed tomography and single-kernel near infrared spectroscopy. *Agriculture and Food Chemistry* 61 10872-10880.

Maize kernel density affects milling quality of the grain. Kernel density of bulk samples can be predicted by nearinfrared reflectance (NIR) spectroscopy, but no accurate method to measure individual kernel density has been reported. This study demonstrates that individual kernel density and volume are accurately measured using X-ray microcomputed tomography (μCT). Kernel density was significantly correlated with kernel volume, air space within the kernel, and protein content. Embryo density and volume did not influence overall kernel density. Partial least-squares (PLS) regression of μCT traits with single kernel NIR spectra gave stable predictive models for kernel density (R2 = 0.78, SEP = 0.034 g/cm3) and volume (R2 = 0.86, SEP = 2.88 cm3). Density and volume predictions were accurate for data collected over 10 months based on kernel weights calculated from predicted density and volume (R2 = 0.83, SEP = 24.78 mg). Kernel density was significantly correlated with bulk test weight (r = 0.80), suggesting that selection of dense kernels can translate to improved agronomic performance.

Joshi, C.P., Thammannagowda, S., Fujino, T. Gou, J., Avci, U., Haigler, C.H., McDonnell, L.M., Mansfield, S.D., Menghesa, B., Carpita, N.C., Harris, D., DeBolt, S., Peter, G.F. 2011.

Perturbation of wood cellulose synthesis causes pleiotropic effects in transgenic aspen. *Molecular Plant* 4: 331-45.

Genetic manipulation of cellulose biosynthesis in trees may provide novel insights into the growth and development of trees. To explore this possibility, the overexpression of a secondary wall-associated cellulose synthase (*PtdCesA8*) gene was attempted in transgenic aspen (*Populus tremuloides L*.) and unexpectedly resulted in silencing of the transgene as well as its endogenous counterparts. The main axis of the transgenic aspen plants quickly stopped growing, and weak branches adopted a weeping growth habit. Furthermore, transgenic plants initially developed smaller leaves and a less extensive root system. Secondary xylem (wood) of transgenic aspen plants contained as little as 10% cellulose normalized to dry weight compared to 41% cellulose typically found in normal aspen wood. This massive reduction in cellulose was accompanied by proportional increases in lignin (35%) and non-cellulosoic polysaccharides (55%) compared to the 22% lignin and 36% non-cellulosic polysaccharides in control plants. The transgenic stems produced typical collapsed or “irregular” xylem vessels that had altered secondary wall morphology and contained greatly reduced amounts of crystalline cellulose. These results demonstrate the fundamental role of secondary wall cellulose within the secondary xylem in maintaining the strength and structural integrity required to establish the vertical growth habit in trees.

Hunter, C.T., Kirienko, D.H., Sylvester, A.W., Peter, G.F., McCarty, D.R., Koch, K.E. 2012. Cellulose synthase-Like D1 is integral to normal cell division, expansion and leaf development in maize. *Plant Physiol*. 158: 708-724.

The *Cellulose Synthase-Like D* (*CslD*) genes have important, though still poorly defined roles in cell wall formation. Here we provide evidence for an unexpected involvement in cell division, broadening the scope of CSLD functions from tip-growing cells to other cell types. Pleiotropic effects of *csld1* maize mutations included narrow, rough-textured leaves, with “warty” lesions of ballooning epidermal cells, some expanding to a 75-fold greater volume than normal. Growth and dry weight of mutant plants was almost 45% less. Although mutant leaves were 35% narrower, epidermal pavement cells were wider, even in non-warty areas, reflecting 45% fewer cells across the blade. Differences in cell-wall composition were not detectable for leaf blades or epidermal peels of *csld1* mutants, but high-resolution X-ray micro CT of stems showed thinner, though denser cell walls. Morphological defects of mutant plants were traced to a narrow temporal and spatial window in early leaf development, co-inciding with highly-localized expression of the *CslD1* gene in the zone of active cell division at the base of leaf blades. In this region, evidence of atypical epidermal cell division included incomplete or erratically positioned cross-walls, and consequent disruptions in cell file organization, cell shapes and sizes, and nuclear dimensions. Flow cytometry confirmed a greater frequency of polyploidy in mutant cells. Collectively, these data indicate a previously un-recognized role for CSLD activity in plant cell division.

SPECIFIC AIM 3: Quantify changes in the distribution of chemical composition induced by pretreatment and during enzyme mediated degradation with MALDI and ion trap

Imaging of lignocellulosic materials requires high molecular specificity to map individual compounds within intact tissue. Although SIMS and MALDI-MS with a single stage of MS have been used to image lignocellulosic biomass, the complexity of the plant tissue limits the interpretation of the mass spectra, making tandem mass spectrometry (MS/MS and MS^n) a more attractive approach. MALDI linear ion trap (LIT) provides MS/MS and MS^n capabilities and thereby delivers the high molecular specificity needed for lignocellulosic analyses. MALDI-LIT MS and MS/MS analyses of cellulose and xylan (hemicellulose) standards were performed to determine mass-to-charge ratios and fragmentation for identification of these compounds in intact tissue. The MALDI-LIT-MS images of young *Populus* wood stem with a single stage of mass analysis suggested an even distribution of both cellulose and hemicellulose ions; in contrast, the MS/MS images of cellulose and xylan generated by plotting characteristic fragment ions resulted in drastically different images. These results clearly demonstrate that tandem MS with the MALDI-LIT is critical for MS analysis of wood tissue to distinguish between isobaric species and to generate accurate imaging of carbohydrates in biomass.

MS of Microcrystalline Cellulose and Hemicellulose Standards. Analyses of purified cellulose and birch xylan extract showed the capability of MALDI-LIT-MS to characterize cellulosic materials, as well as to determine analyte ion *m/z* values to monitor in wood tissue. MCC contains semicrystalline polymers of β-1,4 linked glucose monomers (Glc, $C_6H_{10}O_5$). The neutral molecular weight of cellulose was determined by multiplying the mass of the glucose repeating unit, 162 Da, by the number of glucose monomers and adding 18 to account for the –OH and –H terminal groups. The mass spectrum (*m/z* 500–2000) of MCC displayed ions 162 Da (Glc molecular weight) apart and were identified as sodiated, dehydrated (singly charged) ions, differing by the number of glucose monomers, n, expressed as $[Glc_n\text{-}H_2O+Na]^+$, where n = 3–12. The *m/z* values of MCC ions observed in the MS spectrum are reported in Table 3-1.

Hemicellulose encompasses a variety of different compounds, but 4-O-methylglucronoxylans are the most abundant in wood tissue of angiosperm trees, such as birch and *Populus*. Xylans are composed of a linear β-1,4 linked xylose (Xyl, $C_5H_8O_4$) polymer backbone substituted most commonly with glucuronic acid (GlcA) and 4-O-methylglucuronic acid (MeGlcA) sugars and acetyl groups. The neutral molecular weight of linear xylan polymers was determined by multiplying the mass of the xylose repeating unit, 132 Da by the number of monomers and adding 18 to account for the –OH and –H terminal groups. In the case of substituted xylans, 176 Da and 190 Da are added for GlcA and MeGlcA, respectively. In the mass spectrum (*m/z* 500–2000) of purified Birch xylan extract, ions 132 Da (Xyl residue) apart were observed above the background ions. These ions were identified as sodiated, dehydrated (singly charged) ions of a linear xylan differing by the number of xylose residues, n, in the form $[Xyl_n\text{-}H_2O+Na]^+$, where n = 4–15. The *m/z* values of the most intense xylan ions observed from *m/z* 500-2000 are reported in Table 3-1. In addition to the linear xylans, substituted xylans were observed and further analyzed with MS^2 experiments. MS^2 spectra of the substituted xylans showed a characteristic neutral loss (NL) of 190, which corresponds to molecular weight of MeGlcA, and successive NLs of 132, indicative of xylose residues (data not shown). These ions were identified as a

MeGlcA-substituted xylan and illustrated the ability of MS^2 to differentiate between different xylan ions.

MS and MS^2 of Intact Wood Tissue. Compared to the mass spectrum (*m/z* 500–2000) of cellulose and xylan standards, the mass spectrum from *Populus* wood tissue coated with DHB matrix contains substantially more ions at nearly every *m/z*. Many of these ions are hypothesized to result from the ionization of lignin. Lignin is a complex polymer of polyphenol compounds found primarily in secondary cell walls of gymnosperms, woody angiosperms and grasses, and is abundant in the secondary xylem (wood) of the *Populus* tissue section.[29] To determine the lignin ion signal in intact tissue, lignin was removed from *Populus* wood sections using sodium hypochlorite extraction,[28] leaving behind delignified wood, or holocellulose (composed of cellulose and hemicelluloses), and the sections were analyzed with MALDI-LIT-MS.

Comparing the average spectra of 50 MS scans (*m/z* 500-2000) between untreated and delignified wood from serial sections coating with DHB (Figure 3-1), the total ion current (TIC) was reduced by more than 50% (from $3.08x10^8$ to $1.26x10^8$) and the intensity of the cellulose (analyte) ion signal remained comparable ($2.84x10^5$ compared to $2.55x10^5$). This suggests that the ionization of lignin results in abundant background ion signal in wood tissue; thus, the signal-to-background can be improved by removing lignin from wood tissue. Despite the benefit of improved signal-to-background, removing lignin from wood tissue may alter the wood structure and/or leave behind chemical contaminants, compromising both spatial and chemical information. Instead, the intrinsically high lignin ion signal was effectively reduced by using tandem MS. Tandem MS decreases background signal by isolating ions of interest (removing the remainder of the background ions from the LIT) and increases the signal-to-background ion signal and selectivity of MALDI-LIT-MS imaging experiments.

The *m/z* values of the ions 162 Da apart observed in the MS of the *Populus* stem were consistent with the ions observed in the MS analysis of the MCC standard, suggesting cellulose ions were observed from the MS analysis of wood tissue. MS^2 analyses of the four most abundant ions observed from wood tissue, *m/z* 833, 995, 1157, and 1319 ($[Glc_{4-7}\text{-}H_2O+Na]^+$), were compared to MS^2 of the same ions of the MCC standard (data not shown). The MS^2 spectra from both wood tissue and MCC standard displayed major fragments resulting from glycosidc bond cleavages (sequential neutral losse, NLs, 162), which confirmed cellulose was observed from wood tissue. The MS^2 spectra of the three lowest *m/z* ions (*m/z* 833, 995, and 1157) also displayed an NL of 154 (molecular weight of DHB), suggesting isobaric DHB cluster ions at the same nominal *m/z* values; thus, *m/z* 1319 was used for further analysis of cellulose in wood tissue.

Figure 3-2 compares the MS^2 spectrum of *m/z* 1319 of the MCC standard with the MS^2 spectrum from untreated wood. As expected, both spectra show similar fragmentation—the major fragments (*m/z* 1157, 995, 833, 671, and 509) result from successive NLs of 162, due to glycosidic bond cleavages. Although the major fragment ions of MCC and untreated wood tissue are similar, *m/z* 1319→1301 and 1319→1275 (NLs of 18 and 44, respectively) are more abundant in the MS^2 spectra from wood tissue. The NL of 18 is likely due to a loss of water and

is a non-specific loss, i.e., most ions with an –OH group can lose water during collision-induced dissociation in the ion trap. The NL of 44 from *m/z* 1319 suggests the presence of a acetyl or carboxylic acid functional group, which is common for carbohydrates present in wood tissue, other than cellulose. The greater abundance of these fragments observed in the MS^2 spectrum of untreated wood tissue strongly suggests the presence of at least two isobaric ions at *m/z* 1319.

Figure 3-3 displays the MS^2 spectra of *m/z* 1079 from Birch xylan extract and *Populus* wood tissue. In the xylan standard, sequential NLs of 132 are observed in the MS^2 of *m/z* 1079, resulting from glycosidic bond cleavages between xylose monomers; thus, this ion was identified as $[Xyl_8\text{-}H_2O+Na]^+$. The MS^2 spectrum of *m/*z 1079 from *Populus* tissue shows *m/z* 1079→917 (NL of 162) and 1079→875 (NL of 204), in addition to *m/*z 1079→847 (NL of 132). Since these fragments are not observed in the standard, at least two isobaric ions are likely present at *m/z* 1079. Further stages of MS (MS^3 and MS^4) determined that, in addition to the linear xylan, another ion is present at *m/z* 1079 of the form $[(162)_4(204)_2+Na]^+$, and is preliminarily identified as an O-acetylgalactoglucomannan (another classification of hemicellulose). However, analyses of additional standards such as galactoglucomannan are needed to confirm this preliminary identification.

MS Imaging of Young *Populus* Stem Tissue. MALDI-LIT-MS imaging of intact wood tissue was performed on a quarter section of the *Populus* stem, to ensure that all tissue types were examined. Optical, MS and MS^2 images of a transverse section of young *Populus* stem are displayed in Figures 3-5 and 3-6. The white dotted line in the optical images illustrates the region of MS analysis. The pith is located in the center of the stem and is composed of thin, nonlignified, primary-walled cells. The secondary xylem extends from the pith to the vascular cambium and is composed of living ray parenchyma, as well as nonliving, lignified, fiber and vessel cells with thickened secondary-walls. The vascular cambium is a thin layer (~50 µm) of living tissue between the secondary xylem and secondary phloem where new cells are produced for secondary, or radial, growth. The secondary phloem is composed of living, primary walled parenchyma and companion cells, as well as dead sieve and fiber cells with thickened secondary walls. In contrast to the sieve cells, the fiber walls are lignified.

The mass spectrum of wood tissue (Figure 3-1) displays abundant ion signal at nearly every *m/z* value; however, different tissue regions display characteristic spectra, as displayed in Figure 3-4. For example the periphery of the pith and the secondary phloem, where most live tissue is found, had ions at every *m/z* that were more than 50% greater relative abundance compared with the secondary xylem and middle of the pith where more dead cells are found. On the other hand, abundant ions 162 Da apart (corresponding to ions observed in the MCC standard) were observed above the background ion signal in the secondary xylem and the center of the phloem, corresponding to the thickened secondary walls of the fiber cells. These general differences in the observed spectra were attributed to differences in chemical composition of the various tissues and cell types present in the young *Populus* stem. Although MS analyses are capable of discerning general differences in regions of wood tissue, tandem MS increases the molecular specificity of the experiment to analyze specific analytes in the different regions of wood tissues, as shown in Figures 3-5 and 3-6.

The extracted ion MS image of *m/z* 1319, identified with standards as a cellulose ion [Glc_7-H_2O+Na]$^+$, displays uniform ion signal over all tissue regions of the *Populus* wood stem (Figure 3-5b), as expected because cellulose is present in the walls of all cells. Interestingly, the thin, primary walled cells of the pith and intact vascular cambium (arrow) have similar intensities as the secondary xylem and phloem tissues, even though they are known to contain relatively lower proportions of cellulose.[28] The MS^2 images of *m/z* 1319→1275 and of 1319→995, resulting from NL of 44 and two sequential NLs of 162 (Glc monomers) from the precursor ion, (*m/z* 1319) are displayed in Figure 3-5c and Figure 3-5d, respectively. The MS^2 image of *m/z* 1319→1275 shows the greatest ion signal in the periphery of the pith and secondary phloem. In contrast, the localized ion signal intensity of the MS^2 image of *m/z* 1319 →995 is nearly the inverse, with greater signal in the center region of the pith, the secondary xylem, and small localized regions in the secondary phloem, likely corresponding to fiber bundles known to have greater proportions of cellulose, and the other regions, vascular cambium and secondary phloem without fiber bundles, display less abundant ion signal. Furthermore, the *m/z* 1319→995 ion signal is greater in the older xylem tissue closest to the pith, suggesting this region could have increased cellulose abundance relative to the newer xylem closer to the secondary phloem. However, the difference in cellulose ion signal variation due to inhomogeneous MALDI matrix crystal formation atop the wood tissue needs to be ruled out first. As previously discussed, the MS^2 spectrum of *m/z* 1319 in *Populus* wood tissue (Figure 3-2b) suggests at least two isobaric ions at *m/z* 1319. This was confirmed by comparing the MS image of *m/z* 1319 with the drastically different MS^2 images for *m/z* 1319→1247 and *m/z* 1319→995.

Comparison of *m/z* 1079 (standard analysis identified as a linear xylan ion, [Xyl_8-H_2O+Na]$^+$) MS with the MS^2 images also exemplifies the necessity of tandem MS for wood tissue analyses. Specifically, tandem MS is needed to distinguish between different hemicellulose ions and other interfering ions at the same nominal *m/z*. The extracted MS image of *m/z* 1079 shows nearly even ion signal over the entire tissue section (Figure 3-6b). In contrast, MS^2 images of two fragment ions of *m/z* 1079, *m/z* 947 (NL of 132, 5-carbon sugar), and *m/z* 917 (NL of 162, 6-carbon sugar) have different ion intensities in different tissues and regions. The MS^2 image of *m/z* 1079→947 (Figure 6c) shows higher ion signal localized in the secondary xylem closest to the pith (similar to the cellulose ion intensity), consistent with the hypothesis that this region contains thicker cell walls. The *m/z* 1079→947 ion signal is also observed in the secondary phloem and vascular cambium, which is different than the *m/z* 1319→995 cellulose ion signal. Although no glucuronoxylan is located in the vascular cambium, this region is thinner than the spatial resolution of the imaging experiment. The MS^2 image of *m/z* 1079→917 (Figure 3-6d) shows localized ion intensity in the region of the secondary xylem closest to the pith, but less intense ion signal is observed in the secondary phloem compared to the MS^2 image of *m/z* 1079→947. Moreover, less signal is observed around the pith, which further demonstrates the need for tandem MS to obtain accurate spatial distributions of ions at a single *m/z*.

Although a complete chemical composition analysis of all the regions of wood tissue was not attempted, these experiments show the viability of MALDI-MS^n imaging of lginocellulosic tissue. More specifically, MS alone is incapable of providing accurate spatial distributions of different ions at a single *m/z*. Instead, the necessity and advantages of tandem MS analyses of wood tissue are evident after comparing MS^2 images with the MS images. Specifically, characteristic

fragment ions resulting from collision-induced dissociation of a precursor ion are needed to differentiate between isobaric ions, which are inherent when analyzing carbohydrate composition in complex tissue such as wood. The MS^2 images provide more selectivity for the cellulose and hemicellulose ion signals, differentiate between analytes and interfering ions at a nominal *m/z* value, as well as significantly reduce background ion signal compared to the MS spectrum.

Table 3-1. Mass-to-charge (*m/z*) values of cellulose and hemicellulose ions observed in the MS (*m/z* 500–2000) spectra of microcrystalline cellulose standard and Birch xylan standards. The positive ions were identified as sodiated, dehydrated, singly charged in the form $[Glc_n\text{-}H_2O+Na]^+$ and $[Xyl_n\text{-}H_2O+Na]^+$ for cellulose and hemicellulose, respectively.

Number of Monomers n	**Cellulose Ions $[Glc_n\text{-}H_2O+Na]^+$ *m/z***	**Hemicellulose Ions $[Xyl_n\text{-}H_2O+Na]^+$ *m/z***
3	509	-
4	671	551
5	833	683
6	995	815
7	1157	947
8	1319	1079
9	1481	1211
10	1643	1243
11	1805	1375
12	1967	1507
13	-	1639
14	-	1771
15	-	1903

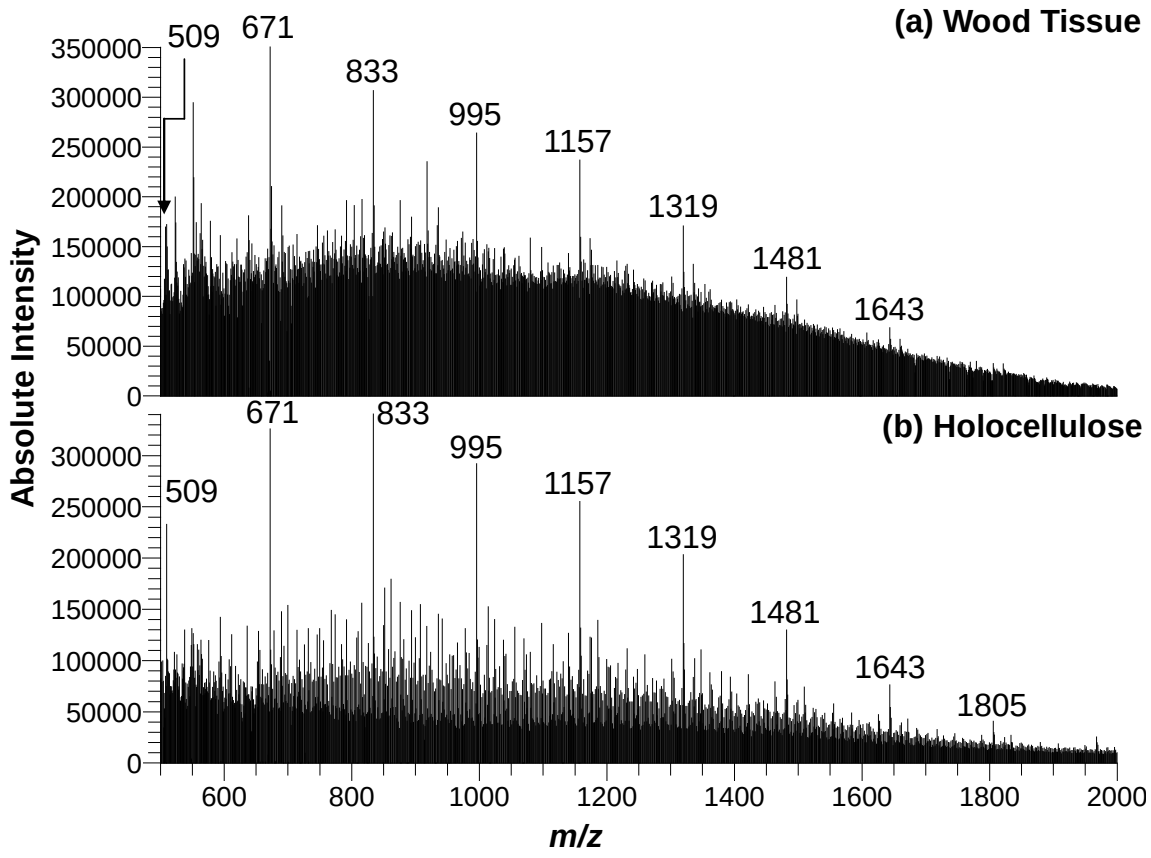

Figure 3-1. Comparison of MALDI MS spectra of intact wood tissue (a) and holocellulose (b). Ions labeled were identified as singly-charged, sodiated dehydrated cellulose ions. Removing the lignin from the wood tissue (leaving behind the cellulose) removes much of the background ion signal, illustrating that many of the ions observed in wood tissue are due to the ionization of lignin.

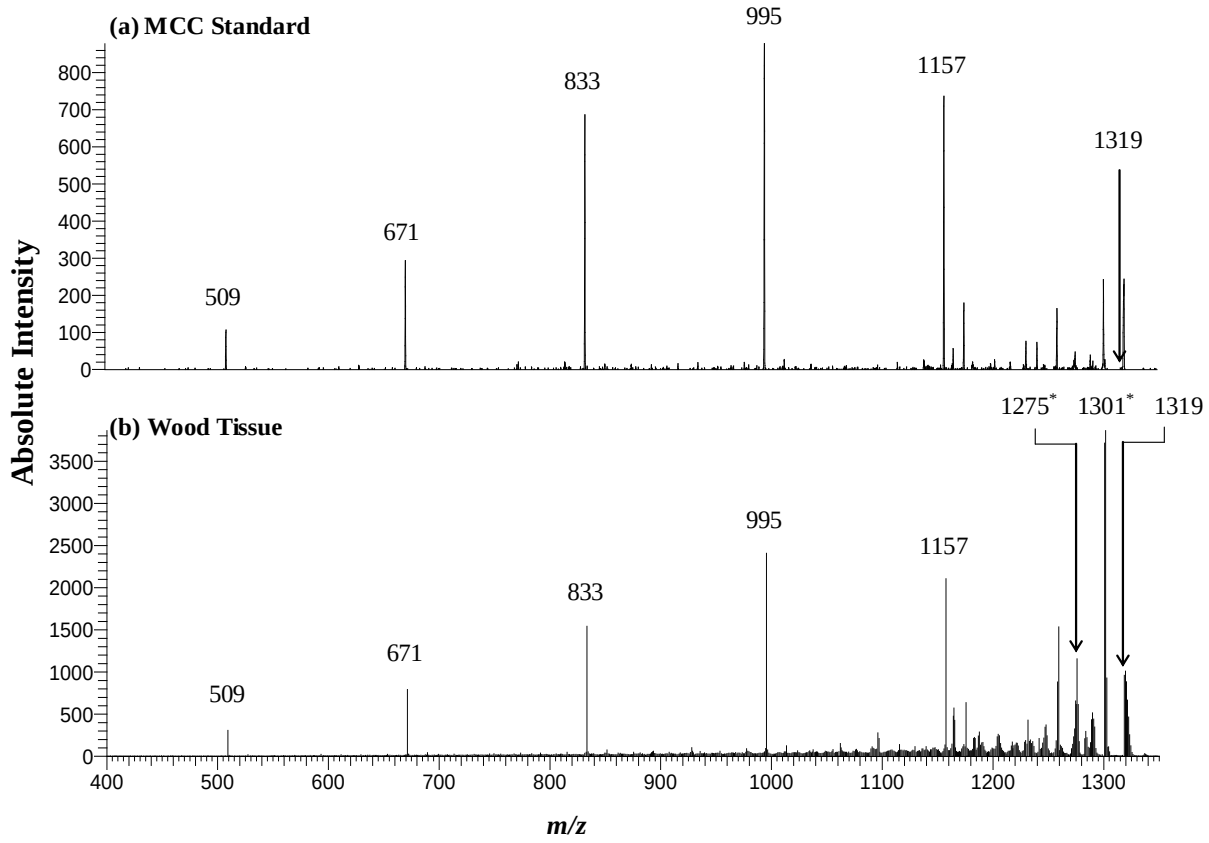

Figure 3-2. MS^2 spectra from MCC standard (top) and intact wood tissue (bottom) of *m/z* 1319, identified as $[Glc_7\text{-}H_2O+Na]_]^+$. Both spectra show abundant fragment ions, arising from successive NLs of 162 resulting from cleavages along the glycosidic bonds. The wood tissue spectrum shows additional fragment ions at *m/z* 1301 and 1275, (NLs of 18 and 44) resulting from loss of water and an an acetyl group, respectively. This suggests at least two isobaric ions are observed from wood tissue at *m/z* 1319. Tandem MS decreases the background compound ion signal (compared with MS in Figure 3-1), improving the signal-to-background ratio without removing lignin.

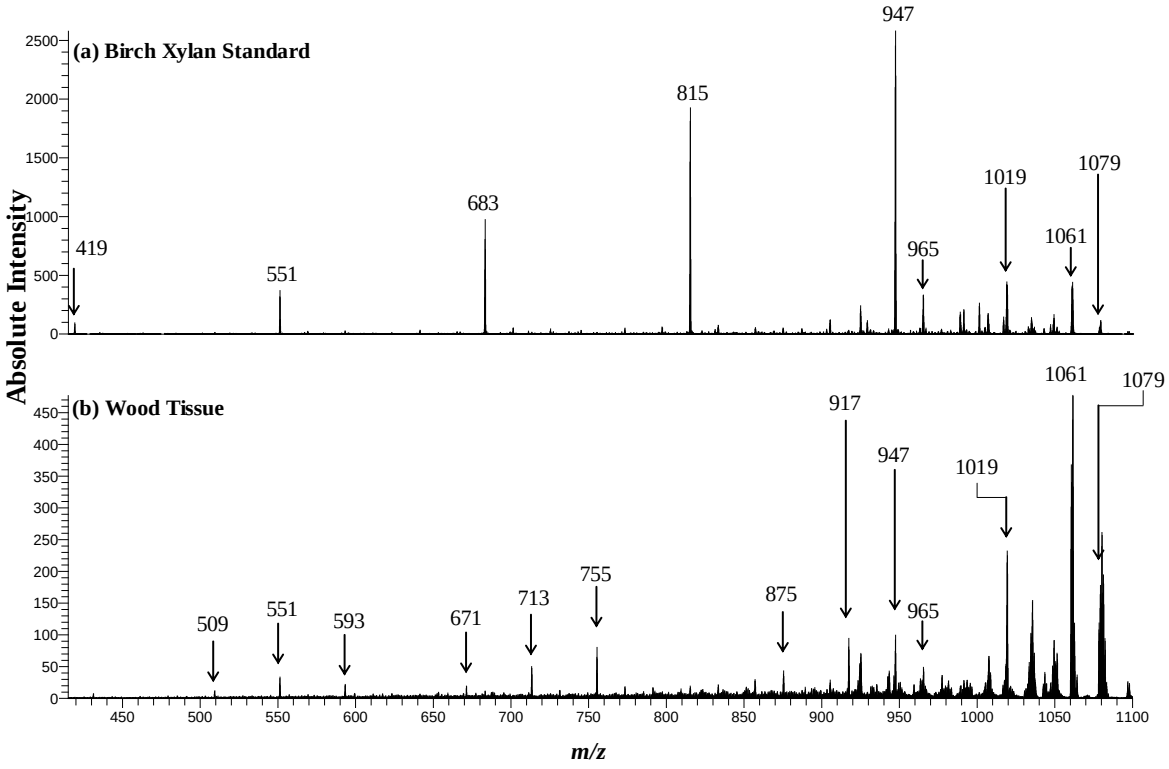

Figure 3-3. MS^2 spectra from Birch Xylan standard (top) and intact wood tissue (bottom) of *m/z* 1079, identified as a linear xylan, $[Xyl_7\text{-}H_2O+Na]^+$. Both spectra show abundant fragment ions at *m/*z 1019 and 947, due to cross ring and glycosidic bong cleavages, respectively. The spectrum from wood tissue also shows abundant fragment ions at *m/z* 917 and 875 (NLs of 162 and 204), corresponding to a glucose and glucuronic acid residue, suggesting at least two isobaric species at *m/z* value 1079.

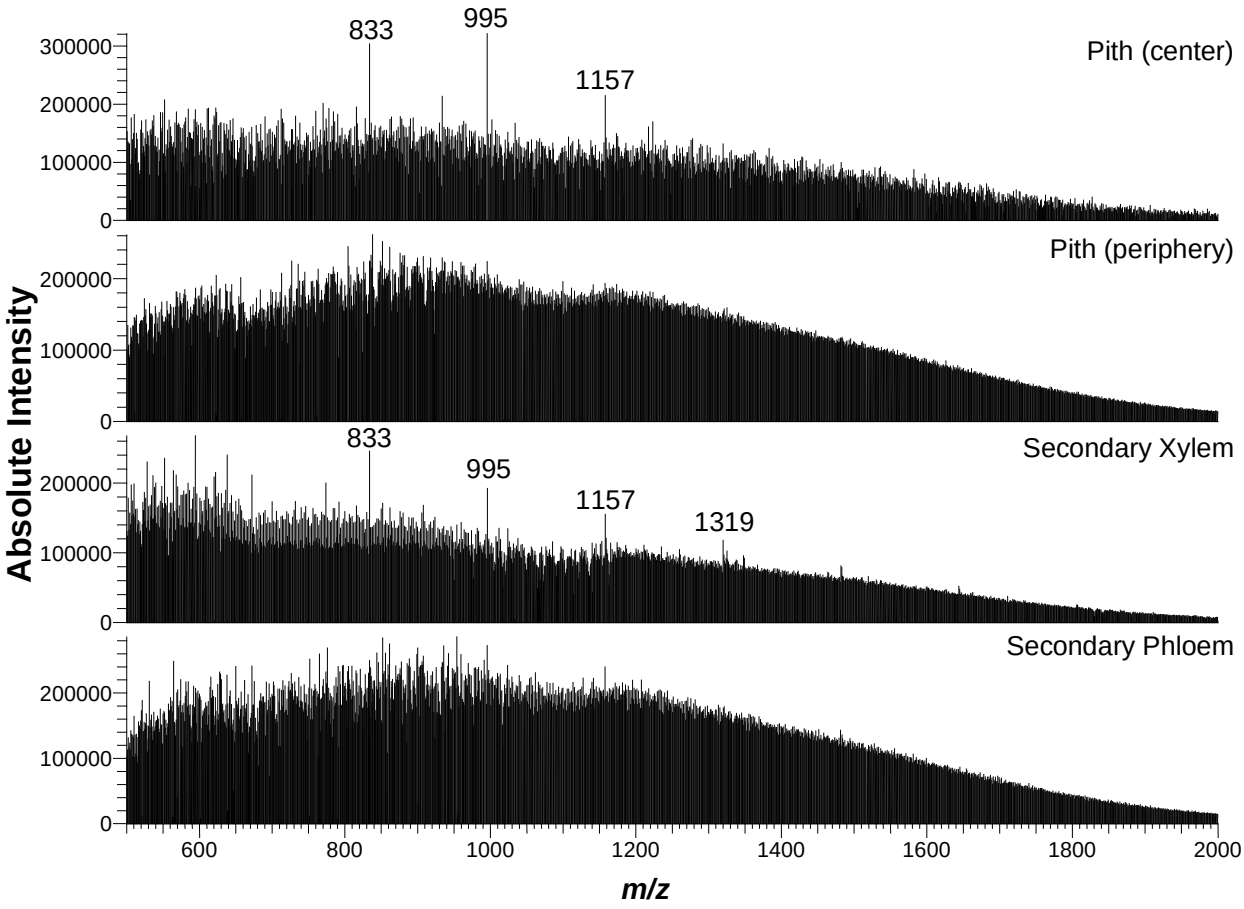

Figure 3-4. Comparison of an average of 25 spectra in four different regions of wood tissue, inner pith, around the pith, secondary xylem, and secondary phloem. Ions above the background, consistent with *m/z* values of MCC, are observed in the spectra of the center pith and secondary xylem. Intense ions at nearly every *m/z* value are observed in the pith periphery and secondary phloem spectra. The differences in spectra are consistent with the composition of the regions: center pith and secondary xylem are composed of mostly dead cells and the pith periphery and secondary phloem are composed of mostly living cells.

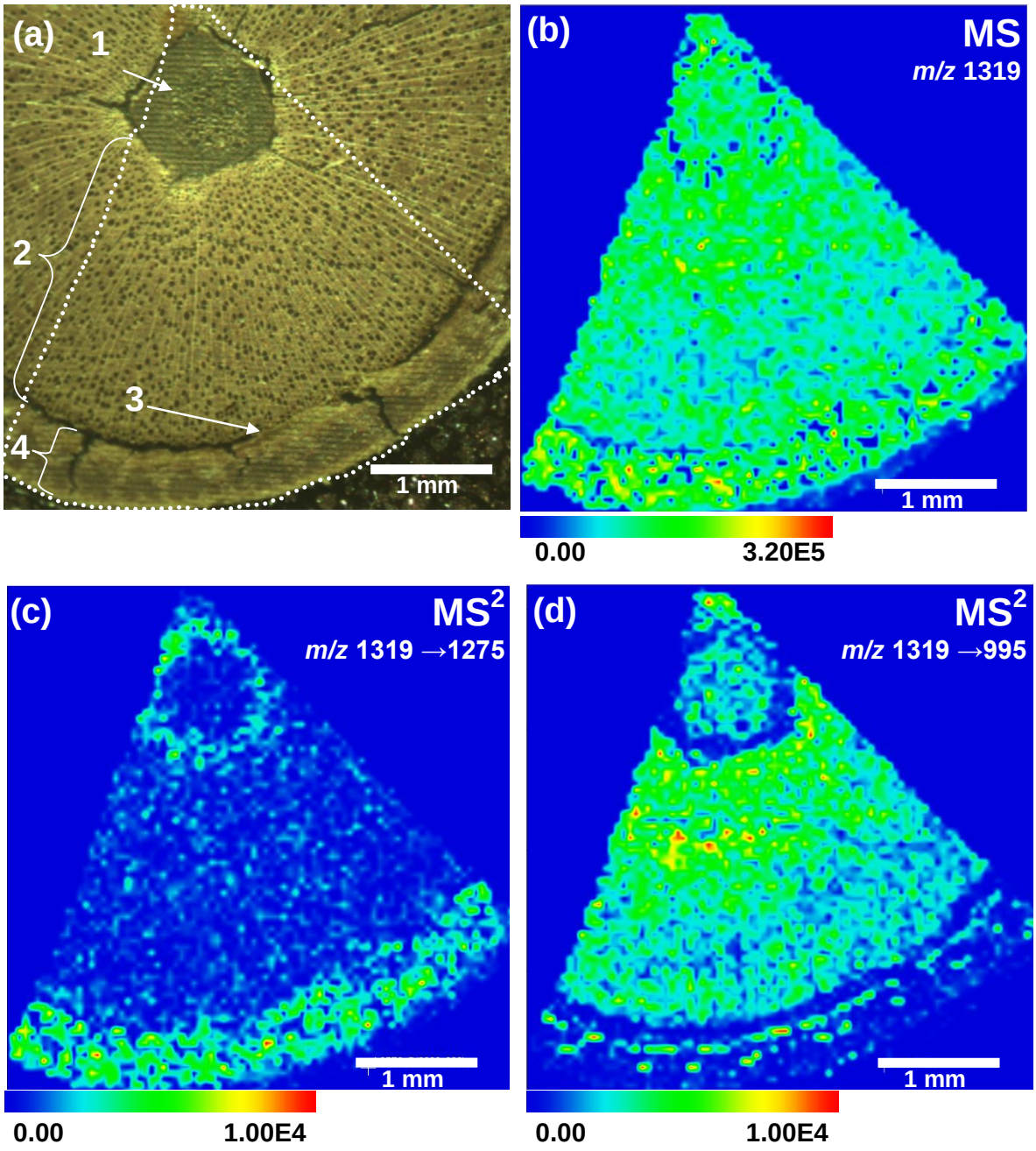

Figure 3-5. (a) Optical image of *Populus* wood tissue showing the pith (1), secondary xylem (2), vascular cambium (3), and secondary phloem (4). The white outline shows the area of MS and MS^2 analyses. (b) MS image of *m/z* 1319 ($[Glc_7\text{-}H_2O+Na]^+$) shows ion signal over the whole tissue. (c) The MS^2 image of *m/z* 1319→1275 (NL of 44) displays more abundant ion signal in the region around the pith and the secondary phloem, which is consistent with tissue compositions. (d) MS^2 image of *m/z* 1319→995, resulting from two NLs of 162, shows localization in the secondary xylem, closest to the pith, and reduced ion signal in the center of the pith, vascular cambium and secondary phloem.

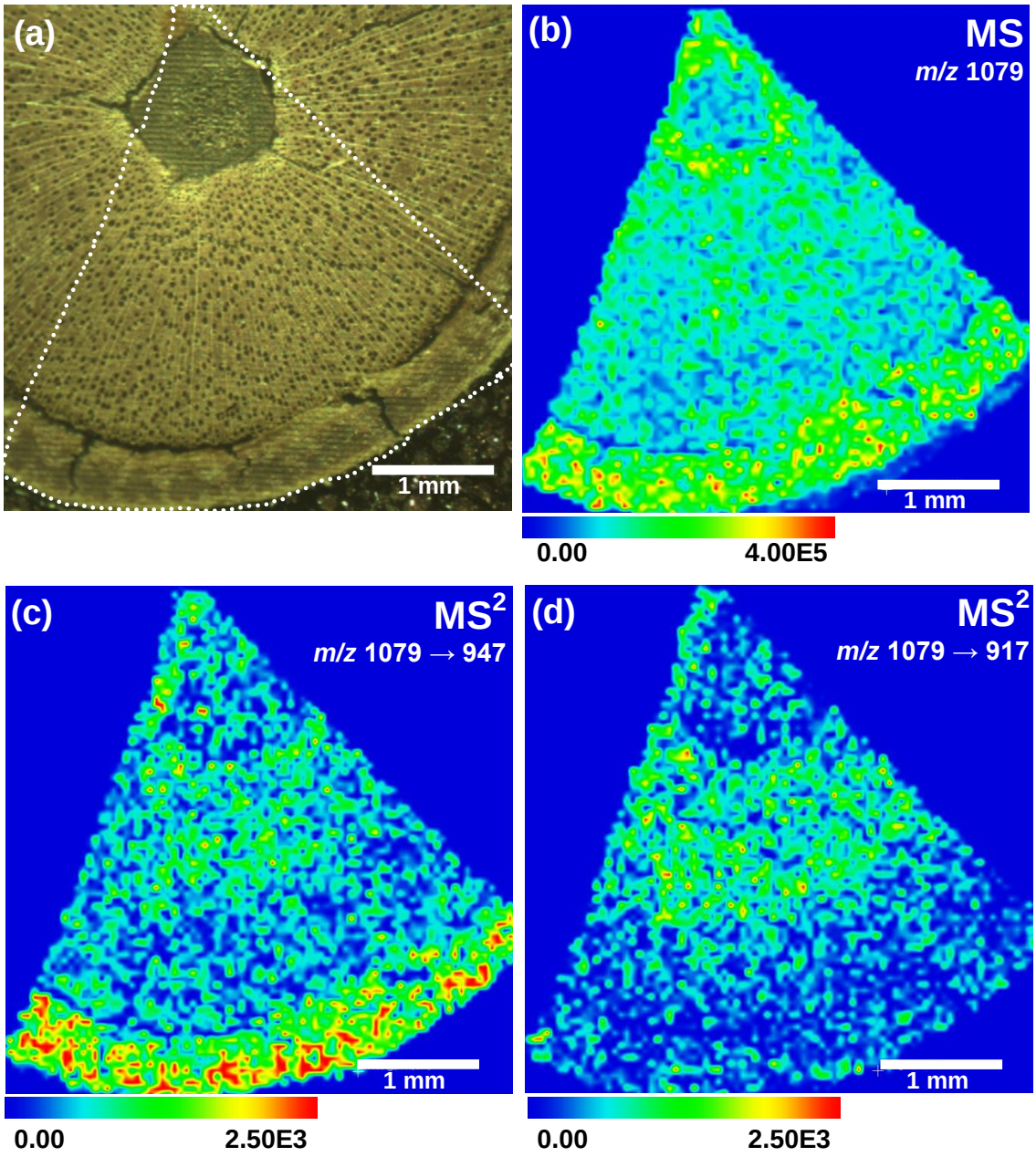

Figure 3-6. (a) Optical image of *Populus* wood tissue with the region imaged outlined in white. (b) MS image of *m/z* 1079 (identified as $[Xyl_7\text{-}H_2O+Na]^+$), shows ion signal over the whole tissue section, with more intensity in the secondary phloem and around the pith. (c) MS^2 image of *m/z* 1079→947 (NL of 132) displays increased ion intensity in the secondary phloem. (d) The MS^2 image of *m/z* 1079→947 (NL of 162) displayed increased ion signal in the secondary xylem closest to the pith. Comparing the MS^2 images of two different fragment ions illustrates that two isobaric compounds are present and that tandem MS can distinguish between them.

MALDI-LIT-MS^n Characterization of Lignin

Since cellulose and hemicellulose were characterized via MALDI-LIT-MS^n previously, experiments exploring lignin characterization were performed. Approximately 20–35% of plant mass is composed of lignin. Unlike hemicellulose and cellulose, lignin does not contain a linear backbone; instead, lignin is a complex 3 dimensional phenolic compound composed of different aromatic alcohols with several different linkages between each monomer. These complex linkages increase the difficulty of structural characterization of lignins. Lignin amount and guaiacyl to syringyl composition is typically analyzed by chemical cleavage and by pyrolysis GC-MS, a technique that breaks down the polymer and the monomer units are analyzed. Lignin can be divided into different categories based on building blocks, for example, S-lignin is primarily composed of syringol units and G-lignin is primarily composed of guaiacuyl units. The difficulty in using MALDI-MS for lignin analyses comes from the similarity of typical MALDI matrices and the building blocks of lignin; however, tandem MS of the LIT provides additional structural information for identification. It was hypothesized that lignin could also absorb at this wavelength, and serve as a MALDI matrix for compounds within wood tissue. Thus, the application of MALDI matrix might be unnecessary.

To test this hypothesis isolated spruce lignin was analyzed with the MALDI-LIT-MS^n method developed in the preliminary stages of this project. **Figure 3-8** shows MS spectra of lignin without matrix and with MALDI matrix (25 mg/mL 2,5-dihydroxybenzoic acid,DHB, dissolved in 0.50 mM sodium acetate). The top spectrum shows lignin is capable of being desorbed and ionized without the addition of MALDI matrix, and also shows the complexity of lignin compounds. Intense ions in the bottom spectrum were further identified as DHB cluster ions, thus the MALDI matrix could be suppressing the ion signal of target analytes. Eliminating the need for MALDI matrix could improve analyses of intact wood tissue, and will be discussed in detail later. **Figure 3-9** shows further characterization of lignin compounds using tandem MS. The MS^2 spectra of *m/z* 151 and *m/z* 181 were identified as vinyl guiacol and vinyl syringol ions, respectively. The major fragment of the vinyl guiacol is a result of neutral loss (NL) of CH_3–OH, which was different from the NL of $H_2C{=}CH_2$ of the vinyl syringol. This shows that MS^n can identify and distinguish between lignin monomer units.

The effects of lignin (and further identification of lignin ions) on MALDI-MS analyses of wood tissue were explored further by removing lignin from wood tissue. Poplar wood tissue was delignified using classical sodium chlorite treatments, leaving behind holocellulose (primarily cellulose and hemicellulose). **Figure 3-10** illustrates the MS^2 image of *m/ z* 181 →121 of untreated poplar wood tissue (top) and holocellulose tissue (bottom). The MS^2 image shows that ion signal is only obtained from the untreated poplar wood tissue, confirming that *m/z* 181 is a lignin ion.

Figure 3-11 shows MS spectra (*m/z* 500–2000) of untreated poplar tissue, holocellulose tissue (from poplar wood), and dilute acid pretreated poplar wood without MALDI matrix application. The three spectra show different characteristics. The untreated wood tissue spectrum shows intense ions above the background that are 162 mass units apart — these *m/z* are consistent with *m/z* values of cellulose standards previously characterized. This suggests that lignin can

act as a MALDI matrix, and desorb/ionize analytes, such as cellulose from wood tissue. The MS spectrum from poplar holocellulose had a ten-fold decrease in ion signal as compared to spectra obtained from untreated and dilute acid pretreated wood. A likely explanation is that removal of lignin, reduces ionization by the laser as there is no compound to absorb energy from the laser and desorb/ionize analyes (specifically, cellulose, which was observed in the untreated wood tissue). Comparing the untreated spectrum with the holocellulose spectrum shows cellulose ion signal is not present; however, numerous ions are still present at nearly every *m/z* ratio, which reiterates the complexity of wood tissue.

The MS of dilute acid pretreated poplar tissue shows increased ion signal in the lower *m/z* range (~500-700) when compared to the untreated wood tissue, and also shows cellulose ions above the background signal (although not as pronounced as the untreated tissue). Dilute acid pretreatment is hypothesized to disrupt the biomass organization without lignin removal. The MS spectrum of the dilute acid pretreated poplar is consistent with this hypothesis, since cellulose ion signal is still observer. Furthermore, the disruption of biomass organization could explain the increase in ion signal, especially in the lower mass region.

Figure 3-12 displays an MS^2 image of *m/z* 1157→833 in dilute acid pretreated poplar wood tissue, holocellulose poplar tissue, and untreated poplar wood tissue (region scanned outlined in blue). The image illustrates how removing lignin dramatically decreases the cellulose ion signal, and dilute acid pretreated wood tissue increases the ion signal, when compared to untreated tissue.

These data clearly show wood tissue can be analyzed without applying MALDI matrix and also, MS and MS imaging shows a change in dilute acid pretreated wood when compared to untreated tissue. However, future experiments will focus on reducing spatial resolution to aim to determine specific spatial changes in specific analytes (e.g., cellulose and lignin), as well as quantifying changes between untreated and pretreated wood tissue.

Untreated Wood Tissue Analyses

Untreated pine wood samples were cryosectioned at ~30 µm in the radial plane and coated with 25 mg/mL 2,5-dihydroxybenzoic acid (DHB). The optical image (Figure 3-13a) shows different regions within the wood tissue: (1) secondary xylem (2) vascular cambial zone and (3) secondary phloem. The secondary xylem and secondary phloem contain non-living cells with thick secondary cell walls composed of cellulose, hemicellulose and lignin. The vascular cambium is a thin layer of living cells with primary walls; thus, that contain reduced amounts of cellulose and no lignin, but have elevated pectin levels.

The MS image of *m/z* 1319(**Figure 3-13b**) normalized to the total ion current (TIC) shows signal over the entire tissue section. Standard characterization of microcrystalline cellulose identified *m/z* 1319 as $[Glc_7\text{-}H_2O+Na]^+$, a cellulose ion. MS^2 image of *m/z* 1319□1157 (**Figure 3-13b**), which results from a neutral loss (NL) of 162 (glucose monomer), displays reduced ion signal in the vascular cambial zone and increased ion signal toward the lower portion of the secondary phloem. Comparing the MS to the MS^2 illustrates that MS^2imcreases the selectivity of the

experiment, and is necessary when trying to analyze on compound in intact wood tissue sections.

Figure 3-14 compares the two MS spectra from the secondary xylem and secondary phloem regions of the wood tissue. Cellulose ions significantly above the background are not observed in the MS of the secondary xylem. The MS of secondary phloem displays cellulose ions above the background, suggesting more cellulose is present relative to the other compounds in the tissue. Future experiments will focus on developing a MALDI-MS^n method to use cellulose ion and background ion intensities to characterize changes in cellulose from laser spot-to-spot, following acid pretreatment at elevated temperatures. In addition, a method to try to quantify cellulose in wood tissue relative to other compounds will be explored.

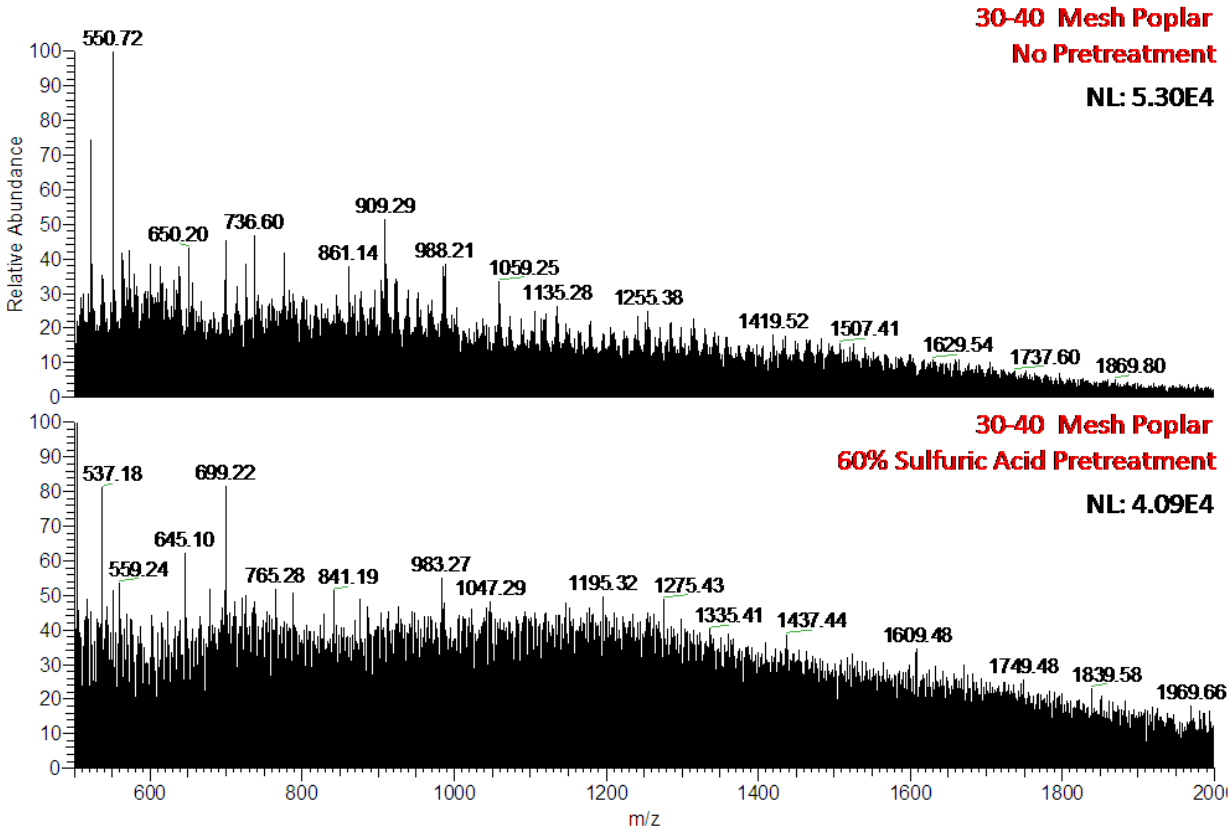

Figure 3-7. Full scan spectra from untreated (top) and pretreated (bottom) 30-40 mesh poplar ground in a tissue grinder. Pretreated spectrum appears to show more intense ions at every mass to charge than the untreated poplar.

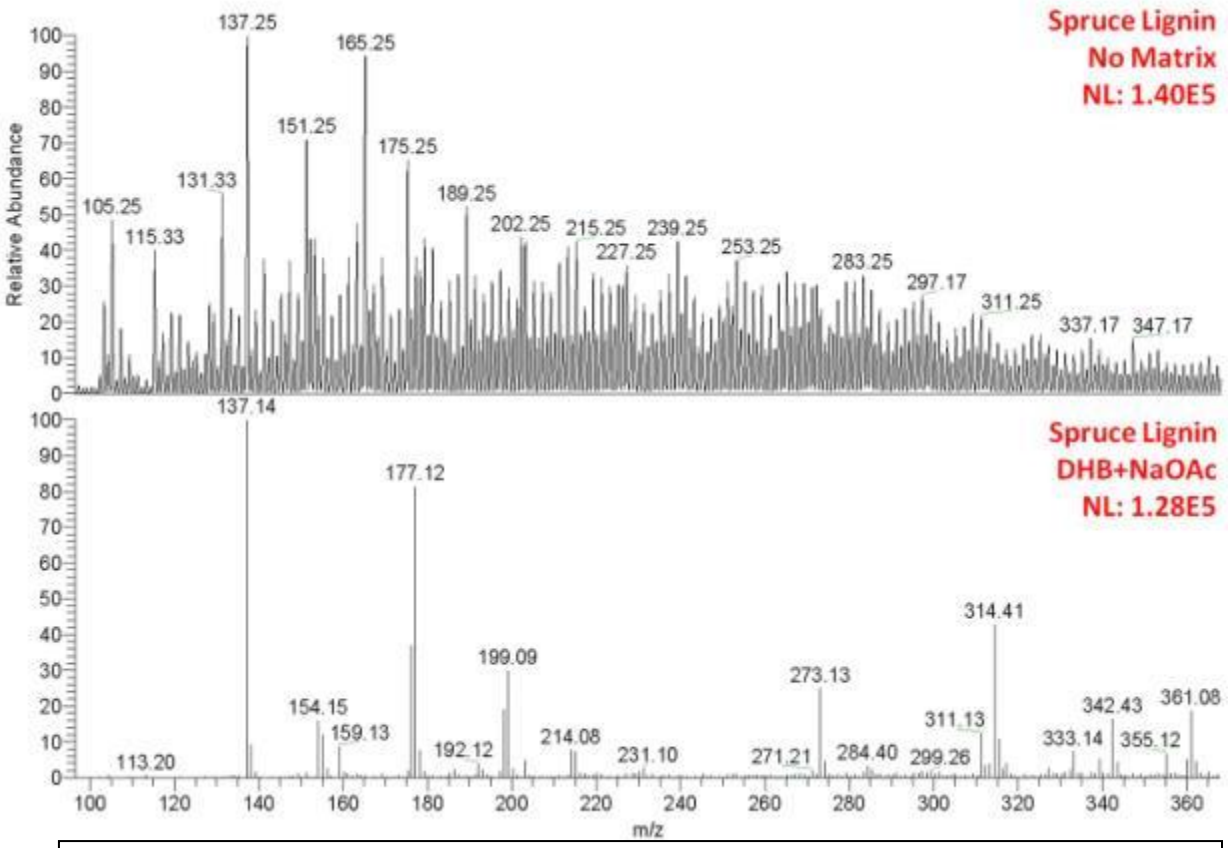

Figure 3-8. MS spectra of Spruce Lignin on stainless steel MALDI sample plate without MALDI matrix (top) with DHB as a matrix. Most m/z in the DHB coated lignin are from DHB, suggesting some suppression of lignin ions by the MALDI matrix.

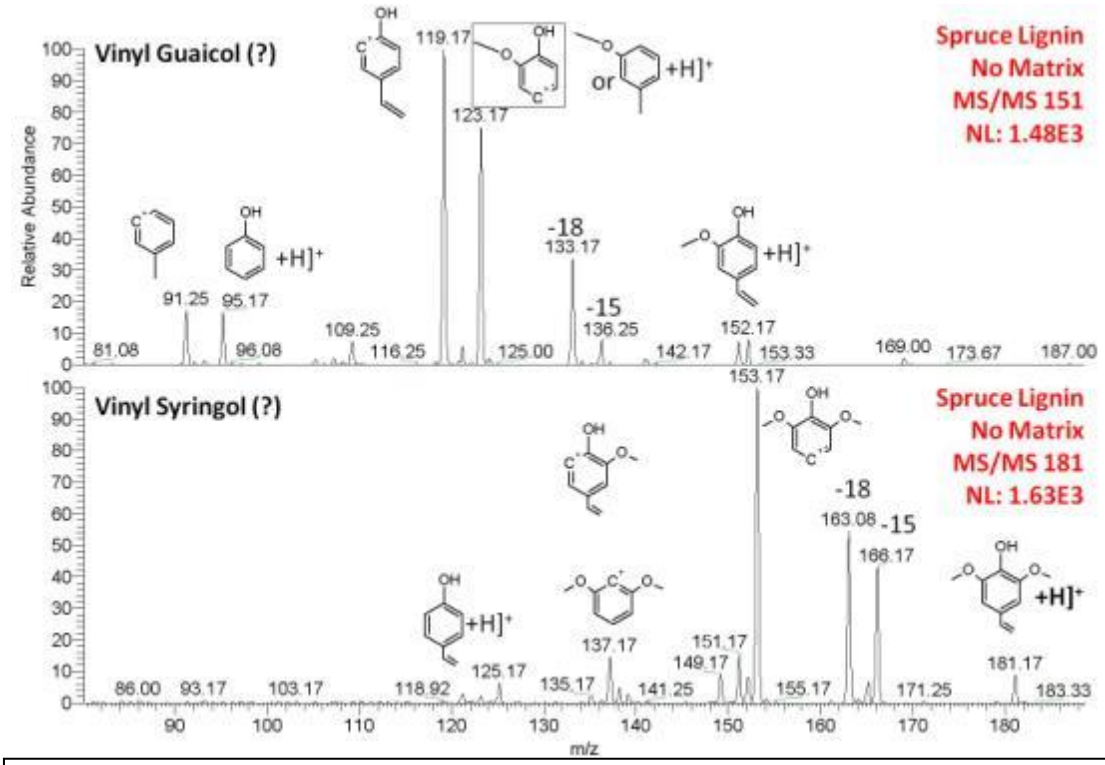

Figure 3-9. MS^2 spectra of Spruce Lignin on stainless steel MALDI sample plate without MALDI matrix. Top shows MS^2 *m/z* 151→ which was identified as vinyl guaicol and the bottom spectrum shows MS^2 of *m/z* 181 → which was identified as vinyl syringol, which are known components of lignin. Fragments are shown in the spectra.

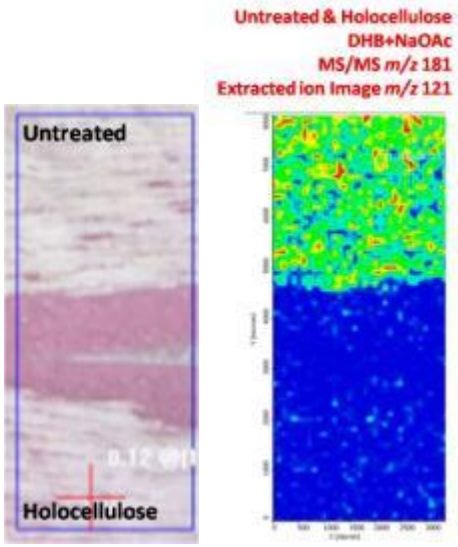

Figure 3-10. Optical image(left) of untreated poplar tissue and holocellulose (poplar) tissue. MS^2 image of *m/z* 181→121, a lignin ion. Image confirms the identification of *m/z* 181 as a lignin ion.

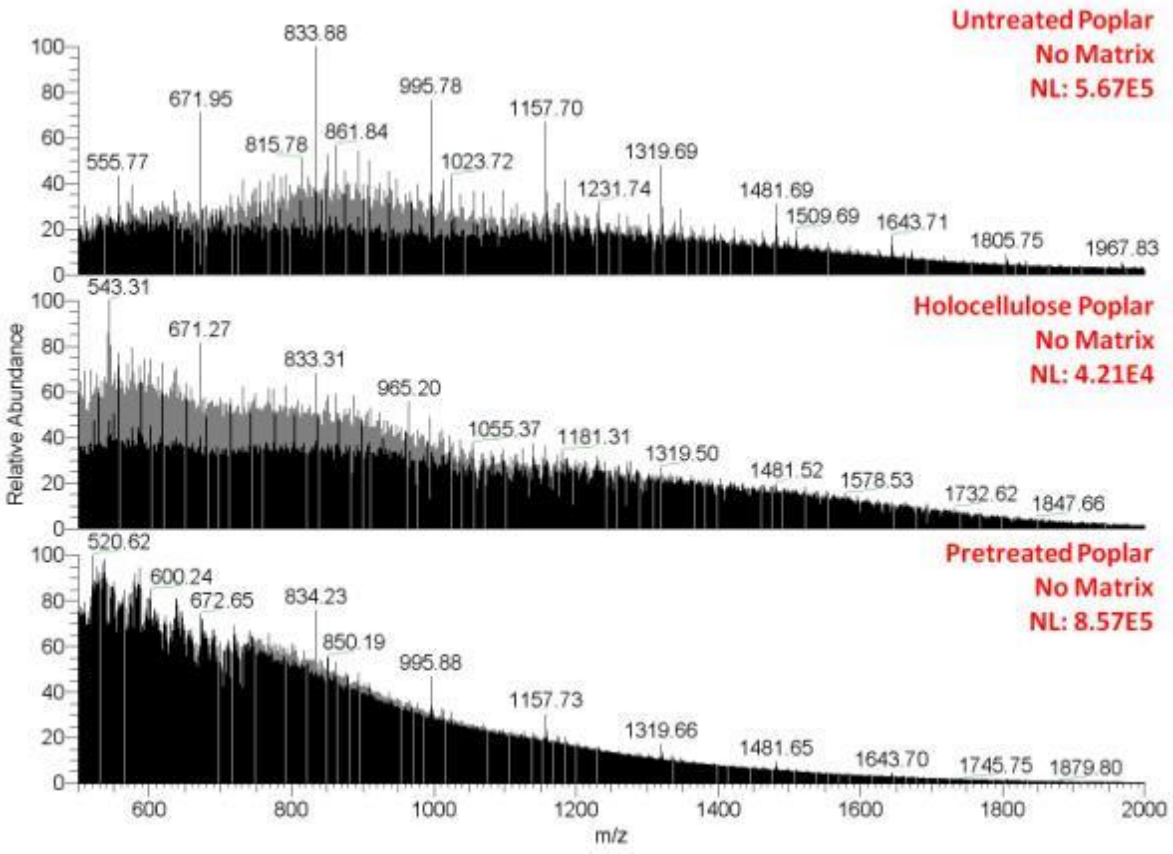

Figure 3-11. Comparison of wood tissue MS spectra without MALDI matrix. MS spectra of untreated poplar (top), delignified poplar (middle) and dilute acid pretreated poplar (bottom) show different characteristics. Note ion intensity of holocellulose is dramatically reduced compared with untreated and pretreated poplar wood.

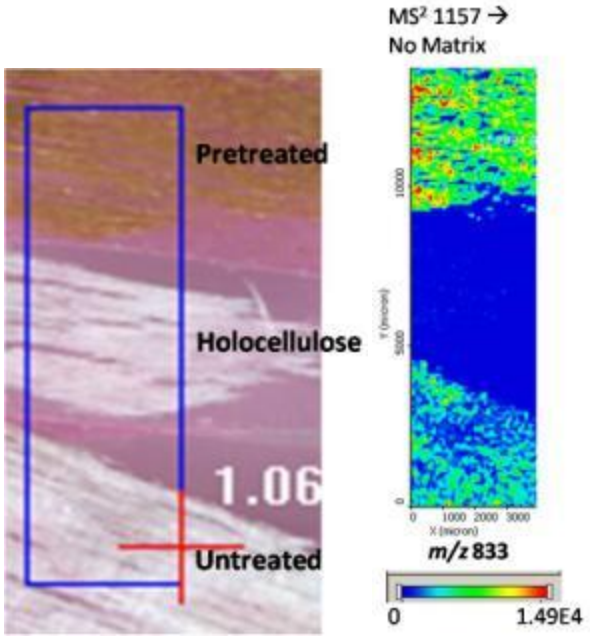

Figure 3-12. Optical and MS^2 image of dilute acid pretreated poplar tissue, holocellulose poplar tissue, and untreated poplar wood tissue. MS^2 image shows extracted ion from *m/z*1157→833, which is a result of two NL of 162 (two glycosidic bond cleavages). Region scanned is outlined in blue on the optical image.

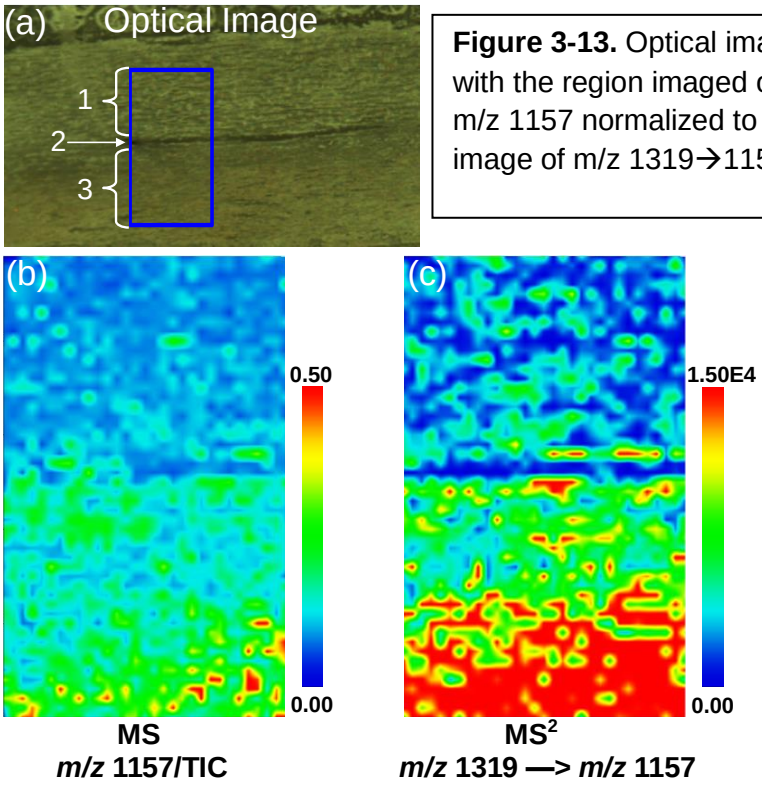

Figure 3-13. Optical image (a) of untreated pine wood, with the region imaged outlined in blue. The MS image of m/z 1157 normalized to the total ion current (TIC) (b). MS^2 image of m/z 1319→1157.

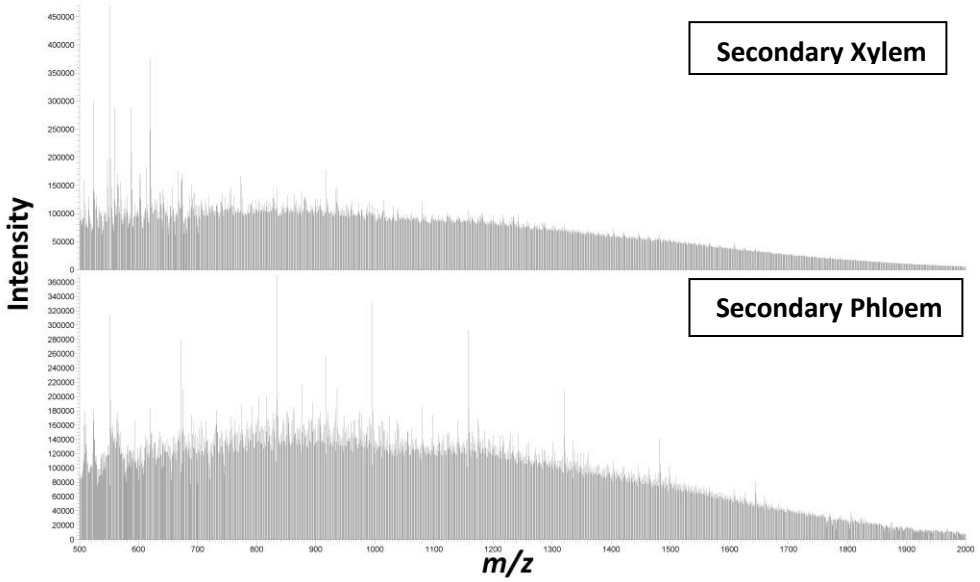

Figure 3-14. Mass spectra (*m/z* 500–2000) of untreated pine wood averaged over the secondary xylem (region 1 in Figure 3-13) and secondary phloem (region 3 in Figure 3-13)

Summary and Future Directions

The analysis of hemicelluloses, cellulose and lignin standards proved useful in trying to analyze wood tissue sections. Large numbers of ions at most every mass are generated in matrix coated and uncoated tissues. MSn is required for imaging to gain the needed specificity for each of the 3 main components of lignocellulosic biomass. Given the overall success of MALDI-LIT-MSn we are working to reduce the area of the laser to 25uM to improve the resolution of our instrument. We are comparing scans before and after MALDI matrix addition. In addition, we are working towards quantitative methods that can be used to estimate the relative distribution of components in pretreated wood. Specifically, more carefully designed experiments of pretreated wood samples could be useful in showing images of the difference in biomass throughout pretreatment. For example, being able to image the depth of penetration of the pretreatment in a wood tissue section could be possible if the pretreatment of the wood tissue is carefully designed.

Lunsford, K.A., Peter, G.F., Yost, R.A., Direct Matrix-Assisted Laser Desorption/Ionization Mass Spectrometric Imaging of Cellulose and Hemicellulose in *Populus* Tissue. 2011. Anal Chem. 83: 6722-30.

Imaging applied toward lignocellulosic materials requires high molecular specificity to map specific compounds within intact tissue. Although secondary ionization mass spectrometry (SIMS) and matrix-assisted laser desorption/ionization-mass spectrometry (MALDI-MS) with a single stage of MS have been used to image lignocellulosic biomass, the complexity of the plant tissue requires tandem MS, which limits the interpretation of simple MS. MALDI linear ion trap (LIT) tandem MS offers the high molecular specificity needed for lignocellulosic analyses.

MALDI-LIT MS imaging analyses of cellulose and xylan (hemicellulose) standards were performed to determine mass-to-charge ratios and fragmentation for identification of these compounds in intact tissue. The MALDI-LIT-MS images of young Populus wood stem showed even distribution of both cellulose and hemicellulose ions; in contrast, the tandem MS images of cellulose and xylan generated by plotting characteristic fragment ions resulted in drastically different images. This demonstrates that isobaric ions are present during MALDI-LIT-MS analyses of wood tissue and tandem MS is necessary to distinguish between isobaric species and accurate imaging of carbohydrates in biomass.

SPECIFIC AIM 4: Integrate the results obtained with the different imaging methods into a preliminary quantitative structural model of how architecture, porosity, chemical organization, composition and structure are changed by pretreatment and enzymatic degradation (*Gary Peter, Alejandro Riveros-Walker, Steve Blackband, Choong Lee, Lonnie Ingram, Kyle Lunsford, Rick Yost*)

Our goal is to integrate the data from MRM, x-ray micro CT and MALDI LIT/MS to develop a more quantitative understanding of the impact of pretreatment on biomass structural properties and the distribution of the main chemical components- cellulose, hemicelluloses and lignin- within the biomass. We have successfully imported and used the analytical software for local thickness evaluations developed for x-ray CT images, with the 3D MRM images. We are scanning exactly the same samples with all 3 imaging methods.

Conclusions from ToF SIMS imaging: Extracted ion images demonstrate the ability of ToF-SIMS to provide high spatial resolution, chemically selective images of intact wood tissue sections. Several ions, although not positively identified, were localized in different regions of tissue and showed high correlated with fluorescence microscopy—these ions can be considered characteristic of these tissue regions to be monitored. Processing (e.g., multivariate analysis) could help to increase the chemical information obtained from ToF-SIMS imaging. The ability to correlate ToF-SIMS images with other imaging techniques will help to provide a more comprehensive analysis of wood tissue. ToF-SIMS imaging provides the spatial resolution needed to provide more insight into spatial changes in chemical composition of pretreated wood tissue.

Figure 1. Optical, fluorescence and positive ion ToF-SIMS images of phloem and xylem of *Populus* wood stem. Images show localization of different ions in different regions of wood tissue. A) Optical image, b) Autofluorescence showing lignin, C) Calcoflur white stain showing cellulose, D) ToF-SIMS total ion count, E) ToF-SIMS m/z 39.0-39.1, F) ToF-SIMS *m/z* 330.7-331.6, G) ToF-SIMS *m/z* 84.8-85.3, H) ToF-SIMS *m/z* 68.9-69.2, J) ToF-SIMS *m/z* 606.7-607.4

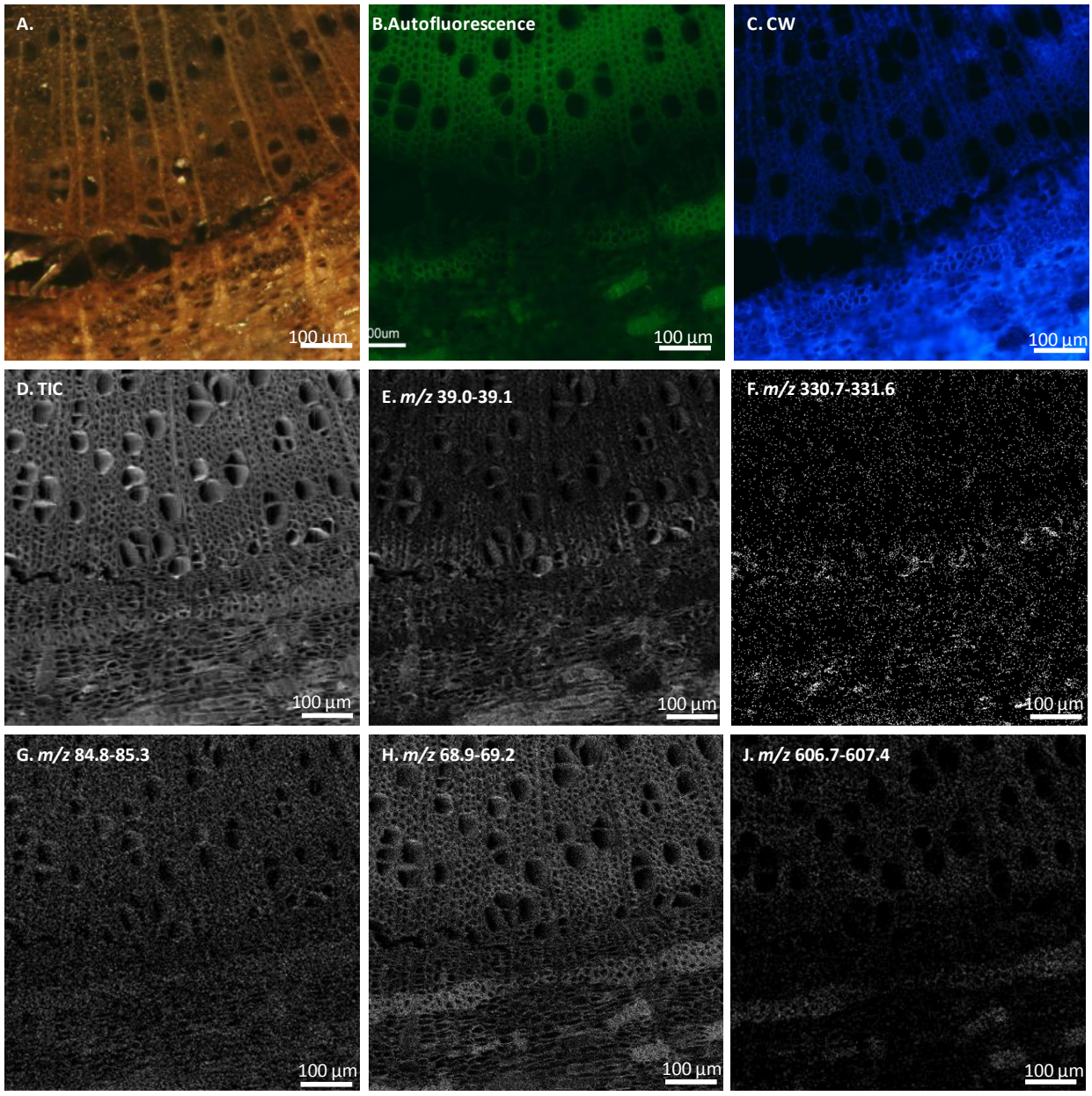

Figure 2. Comparison of different imaging techniques. A) Optical image. B) MALDI-LIT-MS image of a secondary cellulose ion. C) ToF-SIMS image, m/z 68.9 -69.2. D) Calcoflur White fluorescence image. Reducing the raster step size to 10-µm shows intense ion signal in the region of the lignified phloem fibers. Note A and B are images of the same stem. C and D are the same stem, but different from A and B.

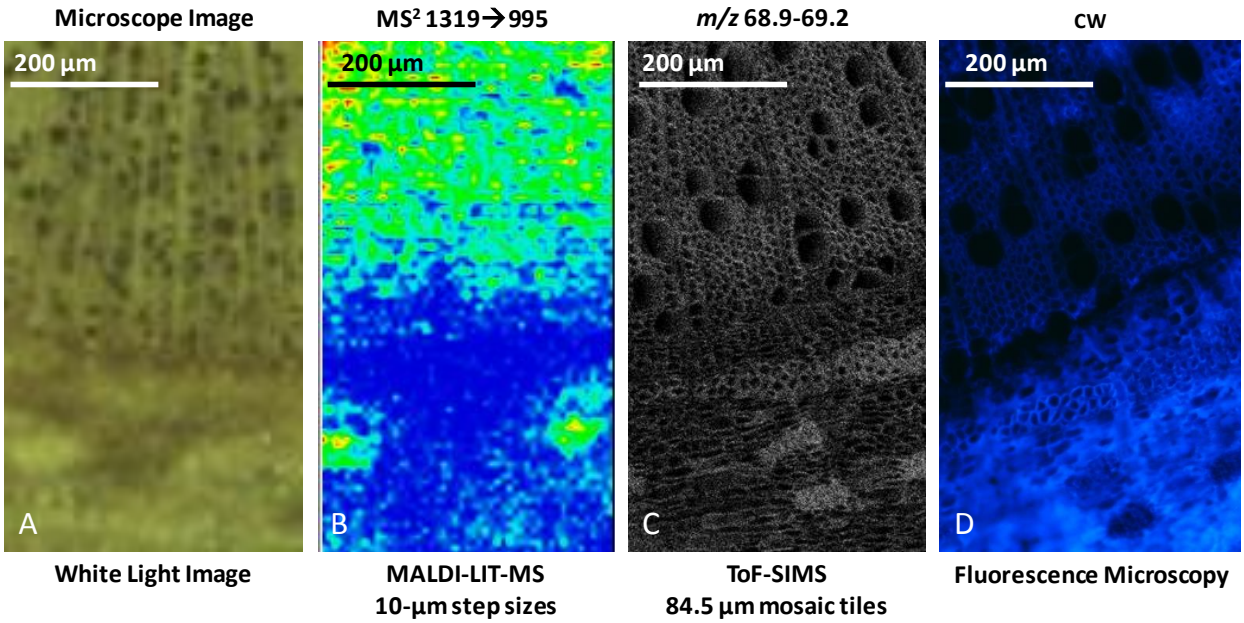

Publications and Presentations

Oral Presentations

Lunsford K.A., Peter, G.F., Yost, R.A., MALDI-LIT-MS^n Imaging Applied To Characterizing Cellulose and Hemicellulose Content in Different Regions of Wood Tissue. NREL, Golden, CO, August, 2012.

Peter, G.F., Lunsford, K.A., Lee, C., Blackband, S., Yost, R.A., Integrated Nondestructive Spatial and Chemical Analysis of Lignocellulosic Materials during Pretreatment and Bioconversion to Ethanol, Bioenergy Science Center Workshop on Biomass Characterization, NREL, Golden, CO, 2011

Kyle A. Lunsford, Gary F. Peter, Richard A. Yost. MALDI Tandem-MS Analyses of Cellulose and Hemicellulose Applied Toward Understanding MS Images of Wood Tissue. Proceedings of the 86th Florida Annual Meeting and Exposition, Innisbrook, FL, May 2010.

Peter, G.F., Lunsford, K.A., Lee, C., Blackband, S., Yost, R.A., Integrated Nondestructive Spatial and Chemical Analysis of Lignocellulosic Materials during Pretreatment and Bioconversion to Ethanol, Bioenergy Science Center Workshop on Biomass Characterization, Riverside, CA, 2010

Poster Presentations

Kyle A. Lunsford, Gary F. Peter, Richard A. Yost. *MALDI-LIT-MS^n Imaging Applied To Characterizing Cellulose and Hemicellulose Content in Different Regions of Wood Tissue,* MP563; Proceedings of the 6th ASMS Conference on Mass Spectrometry and Allied Topics, Denver, CO, June 2011.

Peter, G.F., Lunsford, K.A., Lee, C., Blackband, S., Yost, R.A., Integrated Nondestructive Spatial and Chemical Analysis of Lignocellulosic Materials during Pretreatment and Bioconversion to Ethanol, DOE GTL Awardee IV Workshop, Apr., 2011

Kyle A. Lunsford, Gary F. Peter, Richard A. Yost. *MALDI-LIT-MS^n Imaging Applied To Characterizing Cellulose Content in Different Regions of Wood Tissue,* MP554; Proceedings of the 58th ASMS Conference on Mass Spectrometry and Allied Topics, Salt Lake City, UT, May 2010.

Peter, G.F., Lunsford, K.A., Lee, C., Blackband, S., Yost, R.A., Integrated Nondestructive Spatial and Chemical Analysis of Lignocellulosic Materials during Pretreatment and Bioconversion to Ethanol, DOE GTL Awardee VIII Workshop, Feb., 2010

Peter, G.F., Lunsford, K.A., Lee, C., Blackband, S., Yost, R.A., Integrated Nondestructive Spatial and Chemical Analysis of Lignocellulosic Materials during Pretreatment and Bioconversion to Ethanol, DOE GTL Awardee VII Workshop, Feb., 2009

Kyle A. Lunsford, Gary F. Peter, Richard A. Yost. A Potential for MS Imaging of Cellulosic Tissues is being presented at the 57th ASMS Conference on Mass Spectrometry. 2009

Lee, C., Peter, G.F., Blackband. S.A. 10th International Conference on MR Microscopy (ICMRM) in Montana, August 2009.

Publications

Gustin, J., Jackson, S., Williams, C., Patel, A., Baier, J., Armstrong, P., Edwards, J.W., Peter, G.F., Settles, A.M., 2013. Analysis of maize (Zea mays) kernel density and volume using x-ray micro-computed tomography and single-kernel near infrared spectroscopy. *Agriculture and Food Chemistry* 61 10872-10880.

Hunter, C.T., Kirienko, D.H., Sylvester, A.W., Peter, G.F., McCarty, D.R., Koch, K.E. 2012. Cellulose synthase-Like D1 is integral to normal cell division, expansion and leaf development in maize. *Plant Physiol*. 158: 708-724.

Joshi, C.P., Thammannagowda, S., Fujino, T. Gou, J., Avci, U., Haigler, C.H., McDonnell, L.M., Mansfield, S.D., Menghesa, B., Carpita, N.C., Harris, D., DeBolt, S., Peter, G.F. 2011. Perturbation of wood cellulose synthesis causes pleiotropic effects in transgenic aspen. *Molecular Plant* 4: 331-45

Lunsford, K.A., Peter, G.F., Yost, R.A., Direct Matrix-Assisted Laser Desorption/Ionization Mass Spectrometric Imaging of Cellulose and Hemicellulose in *Populus* Tissue. 2011. Anal Chem. 83: 6722-30.